The Dynamics of Phosphodiesterase Activation in Rods and Cones

Jürgen Reingruber* and David Holcman*†
*Département de Biologie, Ecole Normale Supérieure, Paris, France; and †Department of Mathematics, Weizmann Institute of Science, Rehovot, Israel

ABSTRACT Phototransduction starts with the activation of a rhodopsin (respectively, coneopsin) molecule, located in the outer segment of rod (respectively, cone) photoreceptors. The subsequent amplification pathway proceeds via the G-protein transducin to the activation of phosphodiesterase (PDE), a G-protein coupled effector enzyme. In this article, we study the dynamics of PDE activation by constructing a Markov model that is based on the underlying chemical reactions including multiple rhodopsin phosphorylations. We derive explicit equations for the mean and the variance of activated PDE. Our analysis reveals that a low rhodopsin lifetime variance is neither necessary nor sufficient to achieve reliable PDE activation. The numerical simulations show that during the rising phase the variability of PDE activation is much lower compared to the recovery phase, and this property depends crucially on the transducin activation rates. Furthermore, we find that the dynamics of the activation process greatly differs depending on whether rhodopsin or PDE deactivation limits the recovery of the photoresponse. Finally, our simulations for cones show that only very few PDEs are activated by an excited photopigment, which might explain why in S-cones no single photon response can be observed.

INTRODUCTION

Phototransduction is a multistep process which starts when a photon activates a rhodopsin (respectively, coneopsin) molecule in the outer segment of a rod (respectively, cone) photoreceptor. Upon diffusional encounter on internal disks in rods and on the surface membrane in cones, the activated opsin binds successively to many copies of transducin, a G-protein coupled receptor. Finally, each of the activated transducin binds to a single phosphodiesterase (PDE) effector protein (1–6). The set of activated PDE molecules hydrolyze cGMP, a cytosolic diffusible second messenger, which leads to the closure of cGMP-gated ion channels and thus to the photoreceptor hyperpolarization. In rods, physiological studies have revealed that even the absorption of a single photon can be detected (2,7–9), while for cones, many quasisynchronous absorbed photons (approximately seven) are needed to generate a signal that overcomes the noisy background (10–12). Remarkably, in rods also the single photon response time course is very reproducible (see, e.g., (2)). Despite of major progresses, it is still a challenging problem to unravel the precise mechanisms responsible for the accuracy and reproducibility of the single photon response in rods.

A high reliability of the rod single photon response implies a low variability of the number of activated PDE. This condition can be achieved by controlling accurately the amplification process. Several factors are involved in this amplification, such as the lifetime of activated rhodopsin and the rates of transducin activation. The chemical reactions that control the deactivation of rhodopsin depend on rhodopsin kinase, recoverin, and arrestin (4–6). Recent studies (13–17) have suggested that the reproducibility of the single photon response might be due to a low variability in the lifetime of activated rhodopsin, achieved through rhodopsin deactivation via multiple phosphorylation steps. However, it is still unclear how many deactivation steps are necessary to reproduce the experimental data. In Field and Rieke (14) it was suggested that at least 12–14 steps are needed; however, numerical studies based on Monte Carlo simulations have shown that already seven phosphorylation sites are sufficient to reproduce experimental data (18,19).

To extract the main principles underlying the variability of the photoresponse, we present here a stochastic analysis of PDE activation for both rod and cone photoreceptors. Our model is based on the well-accepted molecular cascade leading to the activation of the G-protein. To analyze the PDE dynamics and the associated fluctuation, we derive equations for the mean and the variance of activated PDE. Since our approach allows us to compute the time course of the mean and the variance of excited PDE, it complements previous stochastic simulations (18,20,21). We derive analytic expressions for the mean and the variance of rhodopsin lifetime and the number of activated PDE, and provide numerical simulations. Furthermore, we study the influence of various parameters such as the number of rhodopsin phosphorylation sites and phosphorylation and transducin activation rates. We explore the impact of the rhodopsin lifetime on the accuracy of PDE activation. We study PDE response for scenarios representing rods and cones in mice and toads. We show that during the rising phase, the PDE variability is much lower compared to the recovery phase. We also analyze the role of whether rhodopsin or PDE lifetimes limit the recovery of the photoresponse. Our results show that the variability of the PDE response depends most significantly on the transducin activation rates. Finally, we present simulations suitable for

Submitted June 26, 2007, and accepted for publication October 17, 2007.

Address reprint requests to David Holcman, E-mail: holcman@biologie.ens.fr.

Editor: Klaus Schulten.

0006-3495/08/03/1954/17 $2.00

doi: 10.1529/biophysj.107.116202

TABLE 1 Parameters used in the model

Symbol	Description
R_n^*	Activated rhodopsin in state n
R_0	Deactivated rhodopsin
T	Transducin
T*	Activated transducin
PDE	Phosphodiesterase
PDE*	Activated PDE
N_p	Number of rhodopsin phosphorylation sites
λ_n	Phosphorylation rate in state n
μ_n	Arrestin binding rate in state n
$k_{act}(n)$	Transducin activation rate in state n
k_3	PDE activation rate
k_4	PDE* deactivation rate
R_τ	Mean/SD ratio of rhodopsin lifetime
R_{Ps}	Steady-state mean/SD ratio of PDE*
$R_P(t)$	Time-dependent mean/SD ratio of PDE*
$\bar{P}_{max}$	Maximum number of PDE*

cones. We find that in cones only very few PDE molecules are activated, which confirms an earlier suggestion (22).

THEORY

Model for PDE activation

The transduction process following the absorption of a photon has been well documented both experimentally and theoretically (for reviews see (1–6)). The Pugh-Lamb model (1,20,23) was based on the properties of two-dimensional random collisions and it predicts accurately the rising phase of the photoresponse. Based on a Markovian approach and using stochastic simulations of diffusion and chemical reactions, in Felber et al. (21), the mean and the variance of the simulated photoresponse were obtained for different lifetimes of activated rhodopsin. We approximate here the different steps leading to PDE activation by first-order chemical reactions and we neglect the molecular dynamics due to diffusion. This approximation is justified by the large number of molecules and the fast diffusion constant. Thus, the number of activated molecules resulting from diffusional collisions has the same temporal law compared to reaction equations.

The well-accepted scenario for PDE activation embodied in our model is the following (see Table 1 for a guide to the parameters used): After a photon absorption, a rhodopsin molecule, denoted by R, undergoes a conformational modification and changes from an inactive into an active form R*. R* deactivation occurs through multiple phosphorylation steps, catalyzed by rhodopsin kinase (RK), and finally through arrestin binding (15,24–27). We take into account that the affinity of R* for transducin, RK, and arrestin are altered by sequential phosphorylations (18,28). The number of rhodopsin phosphorylation sites is denoted by N_p. After photon absorption, rhodopsin changes into the activated state $n = N$. The parameter N equals the total number of R* deactivation steps, and we assume that it is given by $N = N_p + 1$ (13) (number of phosphorylation sites + arrestin binding). When R* encounters RK, with a certain probability a phosphorylation occurs and R* undergoes a transition from the state n to $n-1$, modeled by a state-dependent phosphorylation rate λ_n. When R* binds to arrestin, there is a certain probability that R* becomes deactivated, modeled by a transition rate μ_n from the state n to the deactivated state $n = 0$. In each state $n > 0$, R* activates G-proteins transducin (T) with a rate $k_{act}(n)$. While T* can bind to a PDE with a rate k_3 to form a complex denoted by PDE*, the same complex can be deactivated with a rate k_4. The reciprocal of the rate k_4 is the lifetime of PDE* and depends crucially on the concentration of RGS9 (29–32). We neglect depletion of transducin and PDE because the amount of activated molecules is negligibly small compared to the total pool of available transducin and PDE molecules. The kinetic reactions underlying the model (illustrated in Fig. 1) are summarized as

$$\begin{array}{ccc} R_n^* & \xrightarrow{\lambda_n} & R_{n-1}^* \\ R_n^* & \xrightarrow{\mu_n} & R_0 \\ R_n^* + T & \xrightarrow{k_{act}(n)} & R_n^* + T^* \cdot \\ T^* + PDE & \xrightarrow{k_3} & PDE^* \\ PDE^* & \xrightarrow{k_4} & PDE \end{array} \qquad (1)$$

The model presented in Eq. 1 is a stripped-down version of a more detailed model, such as the one presented in Hamer et al. (18). To keep the model simple and clear, we did not include backward reaction rates. We decided to focus on conditions that can lead to a minimal PDE* variance and therefore omitted backward reaction rates, which would certainly increase the variability of the activation process, as was already noticed in Field and Rieke (14). However, our analysis can be extended without much effort to include backward reaction rates and intermediate bound states between R* and RK. For example, the reactions used to model R* phosphorylation in Eqs. 1a–c in Hamer et al. (18) can be incorporated by using appropriate backward rates λ_n^{-1} (n now labels also intermediate states),

$$R_n^* \underset{\lambda_n^{-1}}{\overset{\lambda_n}{\rightleftarrows}} R_{n-1}^* .$$

In contrast, there is no straightforward method to extend our analysis to incorporate also intermediate bound states between R* and transducin (for example, as modeled by the reactions Eqs. 3a–d in (18)). Indeed, as will be seen later on, our mathematical derivations rely on the assumption that R* deactivation occurs independently from transducin and PDE activation. In this case, the analysis of R* deactivation can be decoupled from the analysis of transducin and PDE activation, which greatly reduces the complexity of the computations. Such a decoupling is justified when the lifetime of possible bound states between R* and transducin is short compared to the lifetime of the phosphorylation states. Since transducin activation occurs much faster compared to R* phosphorylation, we assume that under normal conditions R* deactivation occurs almost independently from transducin and PDE activation.

We now proceed with the analysis of the chemical reactions given in Eq. 1. To describe the state of our model, we introduce three stochastic variables ($\mathcal{N}, \mathcal{L}, \mathcal{K}$) that can adopt the values (n, l, k): the phosphorylation state n of R*, the number l of T*, and k of PDE*. The dynamics of the joint probability

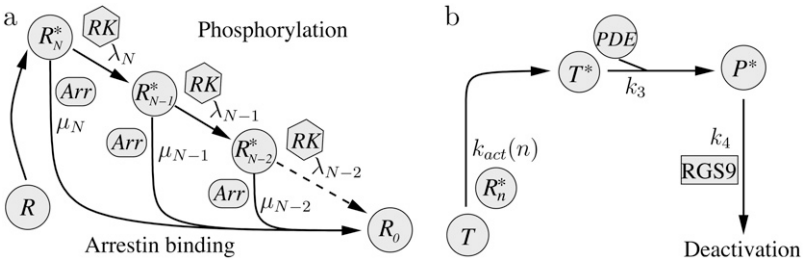

FIGURE 1 Model for PDE activation. (*a*) Activated rhodopsin (R*) can be phosphorylated by rhodopsin kinase (RK) or deactivated by arrestin binding. The phosphorylation rates λ_n and arrestin binding rates μ_n depend on the state n of rhodopsin phosphorylation. Through phosphorylation, R* undergoes a transition from a state n to $n-1$. (*b*) R* in state n activates transducin with a phosphorylation-dependent activation rate $k_{act}(n)$. Activated transducin (T*) binds to PDE with a rate k_3 and forms a complex denoted by PDE*. PDE* is deactivated through RGS9 with a deactivation rate k_4.

$P(n, l, k, t)$, that at time t we find R* in the state n and l T* and k PDE* molecules, satisfies a Master equation (33,34). To derive this equation, we first determine from the system of chemical reactions displayed in Eq. 1 the transition matrix $W(n, l, k|n', l', k', t)$ between two states (n, l, k) and (n', l', k'),

$$\begin{aligned} W(n,l,k|n',l',k',t) = {} & \lambda_{n'}\delta_{n,n'-1}\delta_{l,l'}\delta_{k,k'} + \mu_{n'}\delta_{n,0}\delta_{l,l'}\delta_{k,k'} \\ & + k_{act}(n)\delta_{n,n'}\delta_{l,l'+1}\delta_{k,k'} + \delta_{n,n'}\delta_{l,l'-1}\delta_{k,k'} \\ & + k_3 l'\delta_{n,n'}\delta_{l,l'-1}\delta_{k,k'+1} + k_4 k'\delta_{n,n'}\delta_{l,l'}\delta_{k,k'-1}, \end{aligned} \tag{2}$$

where $\delta_{x,y}$ is the Krönecker delta. From the general shape of the Master equation (33,34)

$$\begin{aligned} & \partial_t P(n,l,k,t|n_0,l_0,k_0,t_0) \\ & \quad = \sum_{n',l',k'} W(n,l,k|n',l',k',t)P(n',l',k',t|n_0,l_0,k_0,t_0) \\ & \quad - P(n,l,k,t|n_0,l_0,k_0,t_0)\sum_{n',l',k'} W(n',l',k'|n,l,k,t), \end{aligned} \tag{3}$$

we obtain, by inserting Eq. 2 into Eq. 3 (we suppress the initial indices (n_0, l_0, k_0, t_0)),

$$\begin{aligned} \frac{\partial}{\partial t}P(n,l,k,t) = {} & \lambda_{n+1}P(n+1,l,k,t) + \delta_{n,0}\sum_{n'=1}^{N}\mu_{n'}P(n',l,k,t) \\ & + k_{act}(n)P(n,l-1,k,t) + \\ & + k_3(l+1)P(n,l+1,k-1,t) \\ & + k_4(k+1)P(n,l,k+1,t) \\ & - (\lambda_n + \mu_n + k_{act}(n) + k_3 l + k_4 k)P(n,l,k,t), \end{aligned} \tag{4}$$

where $N = N_p + 1$. The boundary conditions are

$$\begin{aligned} P(n,l,k,t) &= 0, \text{ if } (n,k,l) < 0 \text{ or } n > N, \\ k_{act}(0) &= 0, \\ \lambda_1 &= 0, \\ \lambda_0 = \mu_0 &= 0. \end{aligned}$$

The conditions $\lambda_0 = \mu_0 = 0$ express that the deactivated state is stable. The condition $\lambda_1 = 0$ accounts for the fact that in the state $n = 1$ all sites are phosphorylated. Immediately after photon absorption, R* is in state $n = N$ and the number of T^* and PDE* are zero. Thus, the initial condition for $P(n, l, k, t)$ is given by

$$P(n,l,k,t=0) = \delta_{n,N}\delta_{l,0}\delta_{k,0}. \tag{5}$$

Dynamics of activated rhodopsin

We now analyze the dynamics of R*. In particular, we estimate the mean and the variance of the duration until R* becomes deactivated by arrestin binding. We start by computing the probability $P(n, t)$ that a R* molecule is in the state n at time t. Our analysis ends with an estimation of the mean to the standard deviation (SD) ratio of R* lifetime.

State probability $P(n, t)$

To describe the dynamics of R*, we sum Eq. 4 over the indices l and k. We obtain an equation for the probability $P(n, t)$ to find R* in the state n at time t,

$$\begin{aligned} & \frac{\partial}{\partial t}P(n,t) \\ & = \begin{cases} -\beta_N P(N,t) & n = N \\ \lambda_{n+1}P(n+1,t) - \beta_n P(n,t) & 1 \le n \le N-1 \\ \sum_{n=1}^{N}\mu_n P(n,t) = \partial_t\left(1 - \sum_{n=1}^{N}P(n,t)\right) & n = 0 \end{cases}, \end{aligned} \tag{6}$$

where $\beta_n = \lambda_n + \mu_n$. The initial condition is given by $P(n, t = 0) = \delta_{n,N}$. Using the vector notation with $\boldsymbol{P}(t) = (P(N,t), \ldots, P(1,t))$, we rewrite this system as

$$\frac{\partial}{\partial t}\boldsymbol{P}(t) = \mathbf{S}\,\boldsymbol{P}(t), \tag{7}$$

where the matrix $\mathbf{S}$ is given by

$$\mathbf{S} = \begin{pmatrix} -\beta_N & & & \\ \lambda_N & -\beta_{N-1} & & \\ & & \vdots & \\ & & \lambda_2 & -\beta_1 \end{pmatrix}. \tag{8}$$

For pairwise different eigenvalues β_n we can diagonalize $\mathbf{S}$ and using the eigenvectors of $\mathbf{S}$ we derive explicit expressions for $P(n, t)$. With the notation $p_i = \lambda_i/\beta_i$, $P(n, t)$ is given by

$$P(n,t) = \left(\prod_{m=n+1}^{N} p_m\right)\sum_{i=n}^{N} e^{-\beta_i t}\frac{\beta_i}{\beta_n}\prod_{\substack{k=n \\ k\neq i}}^{N}\frac{\beta_k}{\beta_k - \beta_i},\ 1 \le n \le N. \tag{9}$$

Mean and variance of rhodopsin lifetime

To compute the mean and the variance of the random R* lifetime T, we use the probability $P_R(t)$ that R* is still active at time t, given by

$$P_R(t) = Pr\{T > t\} = \sum_{n=1}^{N} P(n,t). \tag{10}$$

A direct computation using $P(n, t)$ from Eq. 9 (and the identities in Eq. 71 and Eq. 72) yields for the mean and the variance of the R* lifetime

$$\tau = \int_0^\infty Pr\{T > t\}dt = \sum_{n=1}^{N}\frac{1}{\beta_n}\prod_{k=n+1}^{N} p_k, \tag{11}$$

$$\begin{aligned} \Sigma_\tau^2 &= \int_0^\infty t^2\frac{d}{dt}Pr\{T < t\}dt - \tau^2 \\ &= \int_0^\infty 2t\,Pr\{T > t\}dt - \tau^2 = 2\sum_{n=1}^{N}\sum_{j=1}^{n}\frac{1}{\beta_n}\frac{1}{\beta_j}\prod_{k=j+1}^{N} p_k - \tau^2. \end{aligned} \tag{12}$$

Equation 11 for the mean R* lifetime has an intuitive interpretation: it is the sum of the mean lifetimes in each state n multiplied by the probability to reach this state before being deactivated by arrestin binding.

Reliability of rhodopsin lifetime

We characterize the reliability of R* lifetime by the ratio of the mean to the standard deviation, denoted by R_τ, which is simply the reciprocal of the

coefficient of variation (CV). If R_τ is high (respectively, low), the reliability is high (respectively, low). By using Eqs. 11 and 12, and following the analysis in the Appendix, we obtain the following estimate:

$$R_\tau = CV_\tau^{-1} = \frac{\tau}{\sqrt{\Sigma_\tau^2}} \le \sqrt{N}. \tag{13}$$

The upper limit for R_τ depends only on number of R* deactivation steps N. Based on very general considerations, this result has already been anticipated (16,17). However, by using the explicit formulas we can now study the behavior of R_τ as a function of the underlying rates. Indeed, the maximum value $R_\tau = \sqrt{N}$ is achieved if $\beta_n = const$ and $p_n = 1$ for all n. The condition $\beta_n = const$ conveys that all deactivation states need to have the same lifetime, while $p_n = 1$ is fulfilled if the arrestin binding rates μ_n vanish for all $n > 1$. Thus, the latter condition states that arrestin only binds when R* is in the state $n = 1$ and is therefore fully phosphorylated. This assumption is reasonable, since nonvanishing arrestin binding rates for $n > 1$ effectively reduce the number of deactivation steps and therefore increase the variance.

Mean and variance of the transducin activation rate

The mean and variance of the transducin activation rate are defined as

$$\bar{k}_{act}(t) = \sum_{n=1}^{N} k_{act}(n) P(n,t), \tag{14}$$

$$\Sigma^2_{k_{act}}(t) = \sum_{n=1}^{N} k_{act}(n)^2 P(n,t) - \bar{k}_{act}(t)^2. \tag{15}$$

In principle, the mean and the variance of the activation rate (and any other quantity that depends only on the phosphorylation state of R*) can be computed by using the probabilities $P(n, t)$ given in Eq. 9. However, we will use an alternative method of calculation that relies on differential equations and the decomposition of the activation rate (see below). This method does not require us to explicitly compute $P(n, t)$ and facilitates the derivation of differential equations for the cross-correlation terms (see Eq. 34). We now derive a differential equation for $\bar{k}_{act}(t)$ by differentiating Eq. 14 with respect to time and by using Eq. 7,

$$\frac{d}{dt}\bar{k}_{act}(t) = \sum_{n} k_{act}(n)\partial_t P(n,t) = \sum_{n,m} \mathbf{S}^T_{m,n} k_{act}(n) P(m,t), \tag{16}$$

where $\mathbf{S}^T$ is the transposed matrix of $\mathbf{S}$. To solve this equation, we decompose the vector $\boldsymbol{k}_{act} = (k_{act}(N), \ldots, k_{act}(1))$ into the sum of eigenvectors $\boldsymbol{k}^{(i)}_{act}$ of the matrix $\mathbf{S}^T$,

$$\boldsymbol{k}_{act} = \sum_{i=1}^{N} \boldsymbol{k}^{(i)}_{act}, \tag{17}$$

with

$$\mathbf{S}^T \boldsymbol{k}^{(i)}_{act} = -\beta_i \boldsymbol{k}^{(i)}_{act}. \tag{18}$$

By induction, we obtain for the components of the vectors $\mathbf{k}^{(i)}_{act}$

$$k^{(i)}_{act}(n) = \begin{cases} \sum_{j=1}^{i} k_{act}(j) \left(\prod_{m=j+1}^{n} p_m \right) \frac{\beta_i}{\beta_j} \prod_{\substack{k=j \\ k \neq i}}^{n} \frac{\beta_k}{\beta_k - \beta_i}, & \text{for} \quad n \ge i \\ 0, & \text{for} \quad n < i \end{cases}. \tag{19}$$

The differential equation for the mean of $\boldsymbol{k}^{(i)}_{act}$ is given by

$$\frac{d}{dt}\bar{k}^{(i)}_{act}(t) = \sum_{n,m} \mathbf{S}^T_{m,n} k^{(i)}_{act}(n) P(m,t) = -\beta_i \bar{k}^{(i)}_{act}(t). \tag{20}$$

Using the initial condition that at time $t = 0$ R* is in the state $n = N$ yields

$$\bar{k}_{act}(t) = \sum_{i=1}^{N} \bar{k}^{(i)}_{act}(t) = \sum_{i=1}^{N} \bar{k}^{(i)}_{act}(t=0) e^{-\beta_i t} = \sum_{i=1}^{N} k^{(i)}_{act}(N) e^{-\beta_i t}. \tag{21}$$

Note that the expression for $k^{(i)}_{act}(N)$ provided in Eq. 19 can be verified by comparing Eq. 21 with the result for $\bar{k}_{act}(t)$ obtained by inserting Eq. 9 into Eq. 14.

The variance $\Sigma^2_{k_{act}}(t)$ is calculated analogously to $\bar{k}_{act}(t)$ by decomposing the vector $k^2_{act} = (k_{act}(N)^2, \ldots, k_{act}(1)^2)$.

Mean and variance of activated transducin and PDE

The mean and variance of T* and PDE* are defined as

$$\bar{T}(t) = \sum_{n=0}^{N} \sum_{l=0}^{\infty} \sum_{k=0}^{\infty} l P(n,l,k,t), \tag{22}$$

$$\bar{P}(t) = \sum_{n,l,k} k P(n,l,k,t). \tag{23}$$

Differentiating Eqs. 22 and 23 with respect to time and using the Master equation Eq. 4 yields

$$\frac{d}{dt}\bar{T}(t) = -k_3 \bar{T}(t) + \bar{k}_{act}(t), \tag{24}$$

$$\frac{d}{dt}\bar{P}(t) = -k_4 \bar{P}(t) + k_3 \bar{T}(t). \tag{25}$$

The definitions for the variance and the correlations read

$$\Sigma^2_T(t) = \sum_{n,l,k} l^2 P(n,l,k,t) - \bar{T}(t)^2, \tag{26}$$

$$\Sigma^2_P(t) = \sum_{n,l,k} k^2 P(n,l,k,t) - \bar{P}(t)^2, \tag{27}$$

$$\Sigma^2_{TP}(t) = \sum_{n,l,k} lk P(n,l,k,t) - \bar{T}(t)\bar{P}(t), \tag{28}$$

$$\Sigma^2_{k_{act}T}(t) = \sum_{n,l,k} k_{act}(n) l P(n,l,k,t) - \bar{k}_{act}(t)\bar{T}(t), \tag{29}$$

$$\Sigma^2_{k_{act}P}(t) = \sum_{n,l,k} k_{act}(n) k P(n,l,k,t) - \bar{k}_{act}(t)\bar{P}(t). \tag{30}$$

The equations for the time derivatives of $\sum^2_T(t)$ $\sum^2_P(t)$, and $\sum^2_{TP}(t)$ are given by

$$\frac{d}{dt}\Sigma^2_T(t) = -2k_3\Sigma^2_T(t) + k_3\bar{T}(t) + 2\Sigma^2_{k_{act}T}(t) + \bar{k}_{act}(t), \tag{31}$$

$$\frac{d}{dt}\Sigma^2_P(t) = -2k_4\Sigma^2_P(t) + 2k_3\Sigma^2_{TP}(t) + k_3\bar{T}(t) + k_4\bar{P}(t), \tag{32}$$

$$\frac{d}{dt}\Sigma^2_{TP}(t) = -(k_3+k_4)\Sigma^2_{TP}(t) + k_3\Sigma^2_T(t) - k_3\bar{T}(t) + \Sigma^2_{k_{act}P}(t). \tag{33}$$

To close this system of equations we additionally have to derive differential equations for $\Sigma^2_{k_{act}T}(t)$ and $\Sigma^2_{k_{act}P}(t)$. This is done by using the decomposition of $\boldsymbol{k}_{act}$ given in Eq. 17. We first write

$$\Sigma^2_{k_{act}T}(t) = \sum_i \Sigma^2_{k^{(i)}_{act}T}(t), \quad \Sigma^2_{k_{act}P}(t) = \sum_i \Sigma^2_{k^{(i)}_{act}P}(t). \tag{34}$$

The time derivatives of $\Sigma^2_{k^{(i)}_{act}T}(t)$ and $\Sigma^2_{k^{(i)}_{act}P}(t)$ are derived as

$$\frac{d}{dt}\Sigma^2_{k^{(i)}_{act}T}(t) = -(\beta_i + k_3)\Sigma^2_{k^{(i)}_{act}T}(t) + \Sigma^2_{k^{(i)}_{act}k_{act}}(t), \tag{35}$$

$$\frac{d}{dt}\Sigma^2_{k^{(i)}_{act}P}(t) = -(\beta_i + k_4)\Sigma^2_{k^{(i)}_{act}P}(t) + k_3\Sigma^2_{k^{(i)}_{act}T}(t). \tag{36}$$

The correlations between $\boldsymbol{k}_{act}$ and $\boldsymbol{k}^{(i)}_{act}$, defined by

$$\Sigma^2_{k^{(i)}_{act}k_{act}}(t) = \sum_n k^{(i)}_{act}(n)k_{act}(n)P(n,t) - \bar{k}_{act}(t)\bar{k}^{(i)}_{act}(t), \tag{37}$$

are computed by decomposing the vectors $\boldsymbol{x}_i = (k^{(i)}_{act}(N)k_{act}(N), .., k^{(i)}_{act}(1)\,k_{act}(1))$ into the sum of eigenvectors $\boldsymbol{D}^{(j)}_i$ of the matrix $\mathbf{S}^T$,

$$\boldsymbol{x}_i = \sum_{j=1}^{N} \boldsymbol{D}^{(j)}_i, \quad \text{with} \quad \mathbf{S}^\top \boldsymbol{D}^{(j)}_i = -\beta_j \boldsymbol{D}^{(j)}_i. \tag{38}$$

This yields

$$\Sigma^2_{k^{(i)}_{act}k_{act}}(t) = \sum_j D^{(j)}_i(N)e^{-\beta_j t} - \sum_j k^{(i)}_{act}(N)k^{(j)}_{act}(N)e^{-(\beta_i+\beta_j)t}. \tag{39}$$

In practice, the coefficients $D^{(j)}_i(N)$ are computed numerically by diagonalizing the matrix $\mathbf{S}^\top$. However, by using Eq. 19, also analytic expressions can be derived.

Finally, we define the time-dependent PDE reliability ratio $R_P(t)$ as

$$R_P(t) = CV^{-1}_P(t) = \frac{\bar{P}(t)}{\sqrt{\Sigma^2_P(t)}}. \tag{40}$$

SUMMARY

The explicit expressions for $\bar{k}_{act}(t)$ and $\Sigma^2_{k^{(i)}_{act}k_{act}}(t)$ allow us to close the system of differential equations for the variance of PDE*. This system consists of Eq. 21 and Eqs. 24 and 25 for the mean and Eqs. 31–33, Eqs. 35 and 36, and Eq. 39 for the variances. The simulation results will be obtained by using this close system of equations.

Mean and variance of the total number of activated PDE

It is usually assumed that reliable R* deactivation entails reliable PDE activation (13–16); however, it is worthwhile to have a closer look at the connection between R* lifetime and PDE activation. For this we compute the mean and the variance of the total number of PDE* molecules produced during an single photon response (SPR), obtained by setting $k_4 = 0$, and compare it to the variance of R* lifetime. For vanishing PDE* deactivation rate k_4, after R* shutoff, a steady state will be reached that contains all the PDE* molecules activated during the SPR. In the Appendix we derive expressions for the steady-state mean and variance of PDE*,

$$\bar{P}_s = \sum_{n=1}^{N} \frac{k_{act}(n)}{\beta_n} \prod_{k=n+1}^{N} p_k, \tag{41}$$

$$\Sigma^2_{P_s} = \bar{P}_s + \sum_{n=1}^{N}\sum_{j=1}^{n} \frac{k_{act}(n)}{\beta_n}\frac{k_{act}(j)}{\beta_j} \prod_{k=j+1}^{N} p_k - \bar{P}^2_s. \tag{42}$$

These expressions share similarities with the ones obtained for R* lifetime (Eqs. 11 and 12), since merely $1/\beta_n$ is replaced by $k_{act}(n)/\beta_n$. We define the steady-state reliability ratio R_{Ps}, which corresponds to the reliability of the total number of PDE*, as the ratio of the steady-state mean to the SD. The reliability ratio R_{Ps} is the inverse of the coefficient of variation (CV). In the Appendix we obtain a sharp upper bound for R_{Ps},

$$R_{P_s} = CV^{-1}_{P_s} = \frac{\bar{P}_s}{\sqrt{\Sigma^2_{P_s}}} \le \frac{\sqrt{N}}{\sqrt{1 + \frac{N}{\bar{P}_s}}}. \tag{43}$$

In the case when R* activates many PDE* ($\bar{P}_s \gg N$), the upper limits for R_{P_s} and R_τ are both equal to $\sqrt{N}$. However, it is interesting to examine whether maximal values for R_{P_s} and R_τ can be attained simultaneously. The conditions $k_{act}(n)/\beta_n = const$ and $p_n = 1$ are required such that R_{P_s} achieves its maximum, whereas $\beta_n = const$ and $p_n = 1$ are needed to maximize R_τ. The condition $k_{act}(n)/\beta_n = const$ expresses that, in each state, the same amounts of PDE* have to be activated, whereas $1/\beta_n = const$ requires that each state has the same lifetime. By adjusting the activation rates $k_{act}(n)$, the condition $k_{act}(n)/\beta_n = const$ can be achieved even when the rates β_n are very different. In that case, $R_{\mathbf{Ps}}$ can be maximal while R_τ is far from being maximal. In general, because of the transducin activation rates, maximal values for R_{Ps} and R_τ are not achieved simultaneously, which shows that reliable R* lifetime is neither necessary nor sufficient to achieve reliable PDE activation. Only for constant transducin activation rates, $k_{act}(n) = k_{act}$, the steady-state results for PDE* are determined by the mean and variance of R* lifetime,

$$\bar{P}_s = k_{act}\tau, \tag{44}$$

$$\Sigma^2_{P_s} = \bar{P}_s + k^2_{act}\Sigma^2_\tau. \tag{45}$$

We shall now discuss some aspects of the reliability ratio R_{Ps}, which contains the variability of all the molecular events contributing to PDE activation. R_{Ps} is closely related to the coefficient of variation of the area below the PDE* time response, denoted by CV_{areaP}. In Hamer et al. (18) it was shown that

$$CV_{areaP} = \sqrt{CV^2_{P_s} + \frac{1}{\bar{P}_s}} = \sqrt{\frac{1}{R^2_{P_s}} + \frac{1}{\bar{P}_s}}. \tag{46}$$

It is remarkable that CV_{areaP} depends only on the molecular details involved in PDE activation and not on the PDE* deactivation rate k_4. Consequently, CV_{areaP} does not depend on whether PDE* or R* deactivation limits the recovery of the SPR. For large numbers of activated PDE, it follows that

$$CV_{\text{areaP}} \approx CV_{\text{Ps}}. \tag{47}$$

The coefficient of variation CV_{area} of the area below the SPR current was introduced in Field and Rieke (14). It measures the integrated variability of the SPR: when PDE* dynamics and the SPR current are related by a scaling relationship, we have that $CV_{\text{area}} \approx CV_{\text{areaP}}$ (18), which finally leads to $CV_{\text{area}} \approx CV_{\text{P}_\text{s}}$ (for sufficiently large $\bar{P}_\text{s}$). Consequently, the measured value of CV_{area} can be used to obtain a lower bound of the number of R* deactivation steps (by using Eq. 43). Indeed, experimental results for mutated mouse rods (13) show that CV_{area} behaves approximately like $1/\sqrt{N}$, the limiting behavior of CV_{P_s} (this is the case under the assumption that the number of deactivation steps N correlates with the number of phosphorylation sites N_p through $N = N_\text{p} + 1$). We conclude that CV_{area} is a close measure of CV_{P_s}, but in general, it is not for the coefficient of variation of R* lifetime CV_τ.

RESULTS

Numerical simulations of PDE dynamics

To study the PDE dynamics (mean and variance), we run numerical simulations of Eq. 21, Eqs. 24 and 25, Eqs. 31–33, Eqs. 35 and 36, and Eq. 39. Our aim is to examine the influence of the various parameters on the dynamics of PDE activation.

Choice of parameters

It has been well documented that the time course of the single photon response (SPR) differs substantially between amphibian and mammalian rod photoreceptors (13,14,16, 17,35). In mouse rods, the maximum of the SPR amplitude occurs at ~0.1 s (13,35,36), whereas in toad rods, the maximum of the amplitude occurs at ~1.9 s (16,17). Hence, we decided to run simulations for two different scenarios called Mouse Rod and Toad Rod (see Table 2). Following recent results (35), the mouse rod scenario is characterized by a R* lifetime of 0.080 s and a PDE* deactivation rate of 5 s^{-1}. Unfortunately, as far as we know, similar experimental data is not available for toad rods. To match the time course of the toad rod photoresponse, we chose for the toad rod scenario a R* lifetime of 3 s and a PDE* deactivation rate of 1 s^{-1}. Most important, we chose the toad rod parameters such that, contrary to the mouse rod scenario, recovery is limited by R* lifetime and not by PDE* deactivation. This will allow us to explore the impact of whether rhodopsin R* or PDE* lifetime limits the recovery. To compare simulations, we decided to fix the maximum of the mean number of PDE* $\bar{P}_{\max}$ at a value of 150, as suggested in Leskov et al. (37). It is important to note that for our purpose this value is not critical, because other values will result in a simple scaling. Finally, we chose $k_3 = 50\ s^{-1}$ for the T*-PDE* binding rate (in (18,19) the authors use $k_3 = 200\ s^{-1}$). However, the exact value for k_3 is not very important, as long it is not rate-limiting. Our choice of the parameters is summarized in Table 2.

TABLE 2 Toad rod and mouse rod parameters

	Mouse rod scenario	Toad rod scenario
PDE activation rate (k_3)	50 s^{-1}	50 s^{-1}
PDE deactivation rate (k_4)	5 s^{-1}	1 s^{-1}
Mean rhodopsin lifetime (τ)	0.080 s	3 s
Max. value of $\bar{P}(t)$ ($\bar{P}_{\max}$)	150	150

The PDE deactivation rate and rhodopsin lifetime for the mouse rod scenario are taken from Krispel et al. (35).

Motivated by previous studies (18,28), we consider that transducin activation rates $k_{\text{act}}(n)$ decay exponentially with the number of rhodopsin phosphorylations, that is

$$k_{\text{act}}(n-1) = e^{-\omega_{\text{act}}} k_{\text{act}}(n), \tag{48}$$

where ω_{act} is an adjustable parameter. We also assume that the affinity of rhodopsin kinase for R* decays exponentially with the number of phosphorylations,

$$\lambda_{\text{n}-1} = e^{-\omega_\lambda} \lambda_\text{n}, \tag{49}$$

where ω_λ is also a free parameter.

Since we are interested in conditions leading to the smallest PDE* variance, we will mostly present simulations for a simplified scenario, where the arrestin binding rates μ_n vanish unless R* is fully phosphorylated (which is the case when R* is in the state $n = 1$). Such a scenario is optimal to achieve a high R* deactivation reliability. Furthermore, we choose the arrestin binding rate for $n = 1$ equal to $\mu_1 = e^{-\omega_\lambda}\lambda_2$. When $\omega_\lambda = \omega_{\text{act}}$, this choice ensures that $k_{\text{act}}(n)/\beta_\text{n} = const$ and therefore maximizes the reliability ratio R_{Ps}. Moreover, the choice $\mu_1 = e^{-\omega_\lambda}\lambda_2$ adapts the arrestin binding rate to the phosphorylation rates. In summary, the arrestin binding rates will be chosen as

$$\mu_\text{n} = 0 \text{ for } n \geq 2 \quad \text{and} \quad \mu_1 = e^{-\omega_\lambda}\lambda_2 \text{ for } n = 1. \tag{50}$$

Although we made an effort to decrease the number of free parameters, we still have to specify N, λ_N, $k_{\text{act}}(N)$, ω_λ, and ω_{act}. However, the rates λ_N and $k_{\text{act}}(N)$ are fixed by adjusting rhodopsin's lifetime and $\bar{P}_{\max}$. For given values N and ω_λ, λ_N is determined by rhodopsin lifetime according to Eq. 11. For given values N, ω_λ, and ω_{act} we determine numerically the value of $k_{\text{act}}(N)$ by fixing $\bar{P}_{\max} = 150$. Thus, the remaining parameters that have to be specified are N, ω_λ, and ω_{act}.

Impact of the number of phosphorylation sites

Using the theory developed in the previous section, we now study the impact of the number of R* phosphorylation states on the PDE* response. Such an analysis is particularly rele-

vant, since there are transgenic experiments with reduced number of rhodopsin phosphorylation sites (13,15). We run some simulations for the mean and the variance of PDE* for toad rod parameters and $\omega_\lambda = \omega_{act} = 0.1$. The condition $\omega_\lambda = \omega_{act}$ ensures that the ratio $k_{act}(n)/\beta_n$ values are constant and thus leads to a maximal steady-state reliability R_{Ps} (see Eq. 43). This condition has also been used previously for simulating the photoresponse (18,19).

Fig. 2 *a* shows that during the photoresponse the mean number of T* is very small. Since each T* binds to only one PDE, the number of transducin and PDE molecules that become activated are equal. However, unlike PDE*, T* does not accumulate due to the large rate $k_3 = 50\ s^{-1}$. Contrary to the assumption that during the rising phase the ratio of the number of PDE* to T* is constant (1,3,23), we found by comparing Fig. 2 *a* with Fig. 2 *b* that the time course of PDE* is not proportional to the time course of T*.

We explore in Fig. 2 *c* how the PDE variance decreases with growing number of phosphorylation sites N_p (Fig. 2 *c*). The maximum and the temporal width of the variance both decrease by increasing the number of phosphorylation sites. Additionally, the variance does peak approximately two-times later than the mean and this feature depends only slightly on the number of phosphorylation sites, as it can be observed in Fig. 2 *d*. For six phosphorylation sites, the simulations in Fig. 2 *d* are very similar to experimental recordings for the photocurrent presented in Field and Rieke (14).

Fig. 2 *e* shows the PDE reliability $R_P(t)$ as a function of the normalized mean of PDE*, defined as $x(t) = \bar{P}(t)/\max(\bar{P}(t))$. The value $x = 1$ corresponds to the time to peak of the mean. We decided to plot the reliability ratio $R_P(t)$ as a function of the normalized mean, since this provides a better resolution of the rising phase and additionally shows how $R_P(t)$ changes as a function of the number of PDE* molecules. The horizontal lines in Fig. 2 *e* represent the steady-state values R_{Ps}. Our choice of the parameters implies that R_{Ps} is maximal and approximately equal to $\sqrt{N_p+1}$, see Eq. 43. It is interesting to note in Fig. 2 *e* that during the rising phase, $R_P(t)$ reaches values that are much beyond the steady-state value R_{Ps}. This apparent paradox is a consequence of the activation dynamics and cannot be anticipated from steady-state considerations.

Finally, in Fig. 2 *f* we plot the probability $P_R(t)$ (given by Eq. 10) that R* is activated up to time t. With increasing deactivation steps, R* lifetime becomes less variable and more concentrated around the mean value τ. Moreover, since the decay rate ω_λ is small, the lifetimes of the states n are very similar and therefore R_τ is very close to the optimal value $\sqrt{N_p+1}$ (data not shown).

Transducin activation rates strongly influence the dynamics of PDE activation

To study the impact of the transducin activation and phosphorylation rates, we present in Fig. 3 and Fig. 4 simulations for toad rods, obtained for various decay rates ω_{act} and ω_λ. The number of R* phosphorylation sites is fixed to $N_p = 6$, which is the value found in mouse rods and many other species (13,15,28). If R* activity decays only slightly with subsequent phosphorylations (e.g., $\omega_{act} \sim 0.1$), the PDE* variance peaks nearly twice later than the mean (Fig. 3 *c*) and the ratio $R_P(t)$ at time to peak is much higher than the steady-state ratio R_{Ps} (Fig. 3 *d*). In contrast, Fig. 4, *a–c*, illustrates that the parameter ω_λ, which controls the decay of the phosphorylation rates, does not affect much the dynamics of PDE activation, although ω_λ strongly influences the reliability of R* lifetime (Fig. 4 *d*). We conclude that the behavior of the transducin activation rates is more decisive for the PDE* variance than the variability of R* lifetime.

High activation reliability during the rising phase

We now investigate more closely the time course of the reliability ratio $R_P(t)$ during the rising phase. The simulations depicted in Fig. 2 *e* and Fig. 3 *d* reveal that during the rising phase $R_P(t)$ reaches a maximum that can be much higher than the steady-state value R_{Ps}. Indeed, this behavior follows from the fact that initially the variance and the mean are almost equal (see Eq. 68). As a consequence, as long as the variance and the mean are close, $R_P(t)$ approximately increases like the square root of the mean and, depending on the number of PDE*, can reach values that are much beyond the steady-state limit. At a later time, the variance becomes much larger than the mean and $R_P(t)$ decreases. To show this initial behavior of the variance, we plot in Fig. 5 *a* (respectively, Fig. 5 *b*) the mean to the variance ratio of PDE* corresponding to the set of parameters used in Fig. 2 *e* (respectively, Fig. 3 *d*).

To achieve a high reliability ratio $R_P(t)$ during the rising phase, it is both necessary that the number of phosphorylation sites N_p is large (Fig. 2 *e*) and the transducin activation rates are almost constant (Fig. 3 *d*). Indeed, the main contributions to the PDE* variance during the rising phase are due to the variability of R* lifetime and the variability of the transducin activation rates. The latter can be reduced by choosing ω_{act} close to zero. Increasing the number of phosphorylation sites reduces the variability of R* lifetime, especially for small times. Fig. 2 *f* shows that by increasing the number of phosphorylation sites, a growing initial time-window emerges, during which it is very unlikely that R* becomes deactivated. During this period, the variability of R* lifetime is very low, and in particular much lower than the variability of the whole R* lifetime.

Impact of whether rhodopsin or PDE deactivation limits recovery

In Fig. 6 we present simulations for the mouse rod scenario, where the overall PDE* dynamics is much faster compared to toad rods. In the mouse rod scenario, PDE* deactivation

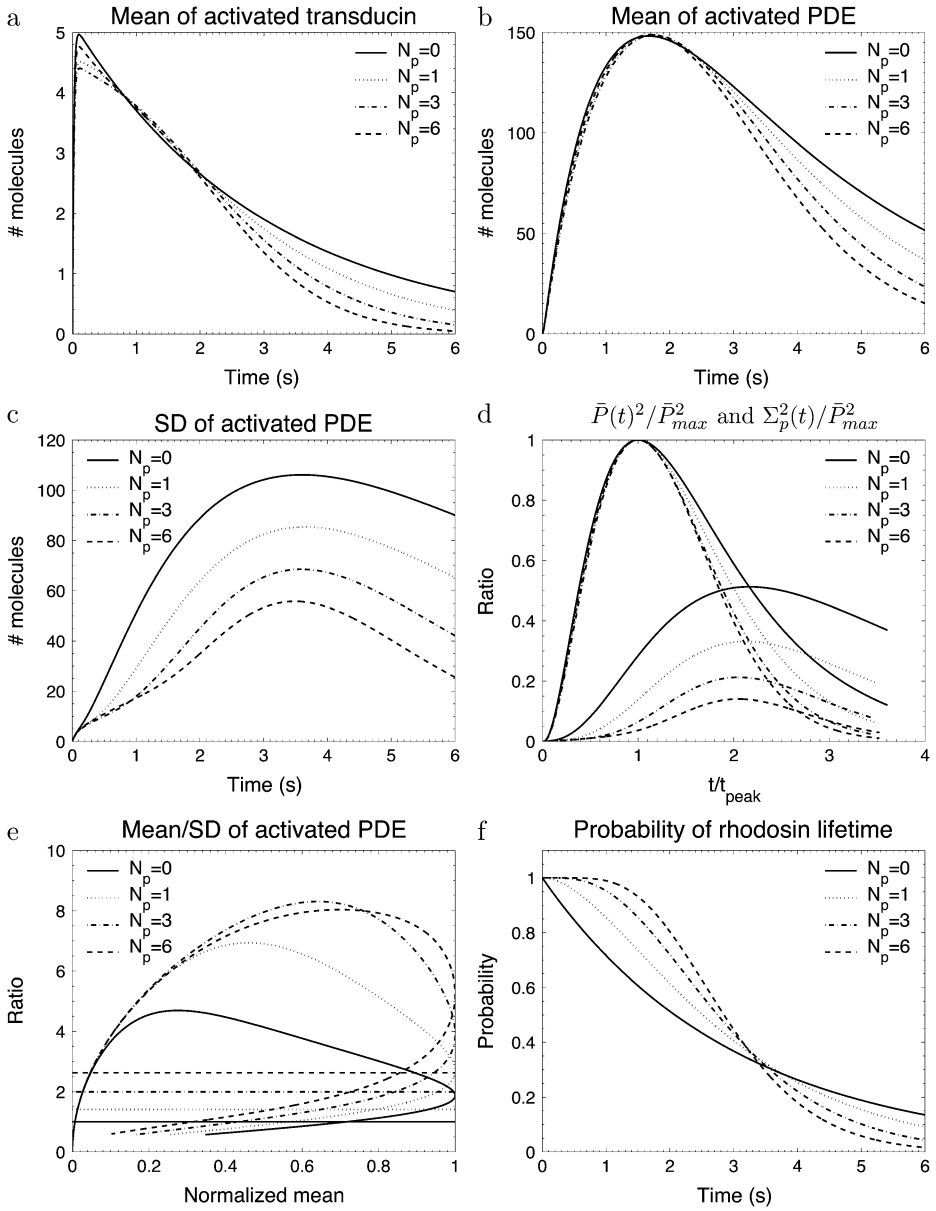

FIGURE 2 The simulations show the impact of the number of rhodopsin phosphorylation sites for the toad rod scenario defined in Table 2. The phosphorylation dependency of the phosphorylation, arrestin binding, and transducin activation rates are given by Eqs. 48–50 with $\omega_\lambda = \omega_{act} = 0.1$. The rates λ_N and $k_{act}(N)$ are adapted to ensure that the rhodopsin lifetime and the maximum number of activated PDE are according to Table 2. For $N_p = (0, 1, 3, 6)$, λ_N and $k_{act}(N)$ are (0.33, 0.70, 1.6, 3.2) s^{-1} and (257, 228, 224, 245) s^{-1}.

limits the recovery, whereas it is R* shutoff in the toad rod case. By comparing the mouse rod simulations in Fig. 6 with the corresponding toad rod simulations in Fig. 3, we conclude that the dynamics of PDE* activation strongly depends on whether R* or PDE* lifetime limits recovery. Consequently, interchanging PDE* and R* lifetime should affect the overall dynamics, as shown by the simulations in Fig. 7. We now examine more closely these two opposing scenarios (see discussion corresponding to Fig. 6 in (18)) where R* deactivation is much faster than PDE* deactivation and then when it is the opposite.

When R* lifetime is much shorter than PDE* lifetime, we can ignore PDE* deactivation during the activation period, and PDE activation and decay occur as two consecutive events. It follows that the peak of the mean number of PDE* occurs at a time when R* becomes deactivated (Fig. 6 *a* and Fig. 7 *a*) and is given by the steady-state value $\bar{P}_s$. The PDE* reliability ratio $R_P(t)$ at the time to peak is given by the steady-state value R_{Ps} (see Fig. 6 *d* and Fig. 7 *d*). Moreover, during the recovery phase, $R_P(t)$ is largely constant and close to R_{Ps}, which can be understood as follows: Since PDE is first activated and then deactivates, during the recovery phase, the mean and the variance of PDE* are given by a decay process with initial values $\bar{P}_s$ and $\Sigma^2_{P_s}$,

$$\bar{P}(t) = \bar{P}_s e^{-k_4 t}$$
$$\Sigma^2_P(t) = \Sigma^2_{P_s} e^{-2k_4 t} + \bar{P}_s e^{-k_4 t}(1 - e^{-k_4 t}).$$

For a timescale smaller than k_4^{-1}, we approximate $\Sigma^2_P(t) \approx \Sigma^2_{P_s} e^{-2k_4 t}$ and thus

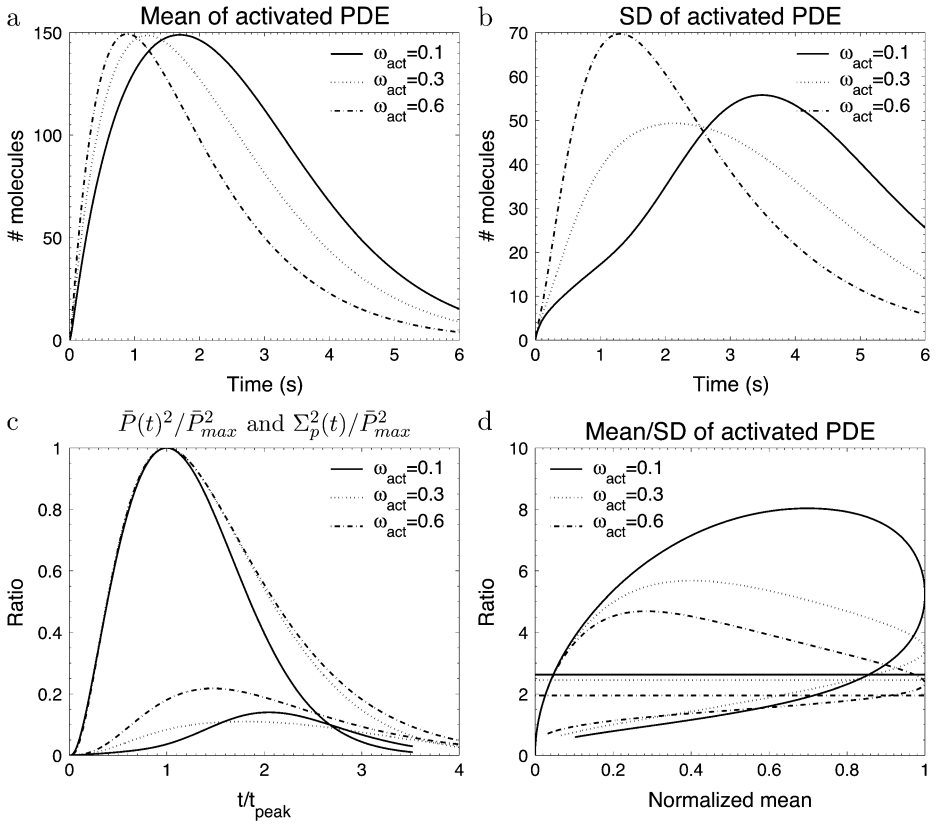

FIGURE 3 The simulations show the impact of the phosphorylation dependency of the transducin activation rates for the toad rod scenario defined in Table 2. The behavior of the phosphorylation, arrestin binding, and transducin activation rates are given by Eqs. 48–50 with $\omega_\lambda = 0.1$ and $N_p = 6$. For $\omega_{act} = (0.1, 0.3, 0.6)$ the rates λ_N and the $k_{act}(N)$ are given by (3.2, 3.2, 3.2) s^{-1} and (245, 356, 482) s^{-1}.

$$R_P(t) = \frac{\bar{P}(t)}{\sqrt{\Sigma_P^2(t)}} \approx \frac{\bar{P}_s}{\sqrt{\Sigma_{P_s}^2}} = R_{P_s}.$$

The times to peak of the PDE* mean and variance are close (Fig. 6 *c* and Fig. 7 *c*). If we define the duration of the PDE* response as the time until all the PDE* molecules become deactivated, then, for large $\bar{P}_s$, the mean duration increases logarithmically with the number of PDE* as $k_4^{-1}\ln(\bar{P}_s)$. Using some computations, it can be shown that the CV of the duration decreases logarithmically with $\bar{P}_s$. We conclude that the duration of the response becomes more and more reliable with increasing number of PDE*, but the CV of the duration is not zero (see also (18)).

When R* lifetime is much larger compared to PDE* lifetime, because PDE activation and deactivation occur simultaneously, unexpected effects are generated. In that case, the PDE* reliability at time to peak can be much higher than the steady-state ratio R_{P_s} (Fig. 7 *d*). However, since the ratio $R_P(t)$ cannot grow faster than $\sqrt{\bar{P}(t)}$ (see Eq. 70), the reliability at time to peak remains bounded by $\sqrt{\bar{P}(t_{peak})}$. Consequently, the CV of the amplitude cannot become zero (see (18)). Even for constant R* activity k_{act}, a steady state is reached with $\bar{P} = k_{act}/k_4$, $\Sigma_P^2 = \bar{P}$ and thus the CV is given by $1/\sqrt{\bar{P}}$. If R* deactivation is rate-limiting, the duration of the PDE* response is determined by R* lifetime and the CV of the duration is given by CV_τ in Eq. 13, which can be very different from CV_{areaP}. Most of the variability is generated during the recovery phase, which causes the variance to peak much later than the mean (Fig. 7 *c*).

Finally, Fig. 7 *d* reveals that there is a tradeoff between the reliability during the rising and recovery phase: the higher the reliability during the rising phase, the lower the reliability will be during the recovery phase. To analyze this behavior, we remark that CV_{areaP} is independent of what rate limits recovery (see Eq. 46) and depends only on the number of phosphorylation sites. Thus, CV_{areaP} is identical in both scenarios presented in Fig. 7 *d*. Now, if R* lifetime limits the recovery, the PDE* reliability during the rising phase is high, which implies a low area variability in this phase. Consequently, the reliability of PDE* during the recovery phase has to decrease (which implies a higher area variability in this phase) to ensure the overall value for CV_{areaP}.

Influence of arrestin binding rates

We now examine the impact of linearly and exponentially increasing arrestin binding rates. In the previous simulations, we allowed arrestin to bind only when R* was fully phosphorylated. For a given number of phosphorylation sites, this condition is optimal to minimize the variance. However, experimental results indicate that arrestin already weakly binds before R* is fully phosphorylated. Biochemical data (28) suggested that arrestin binds only to phosphorylated

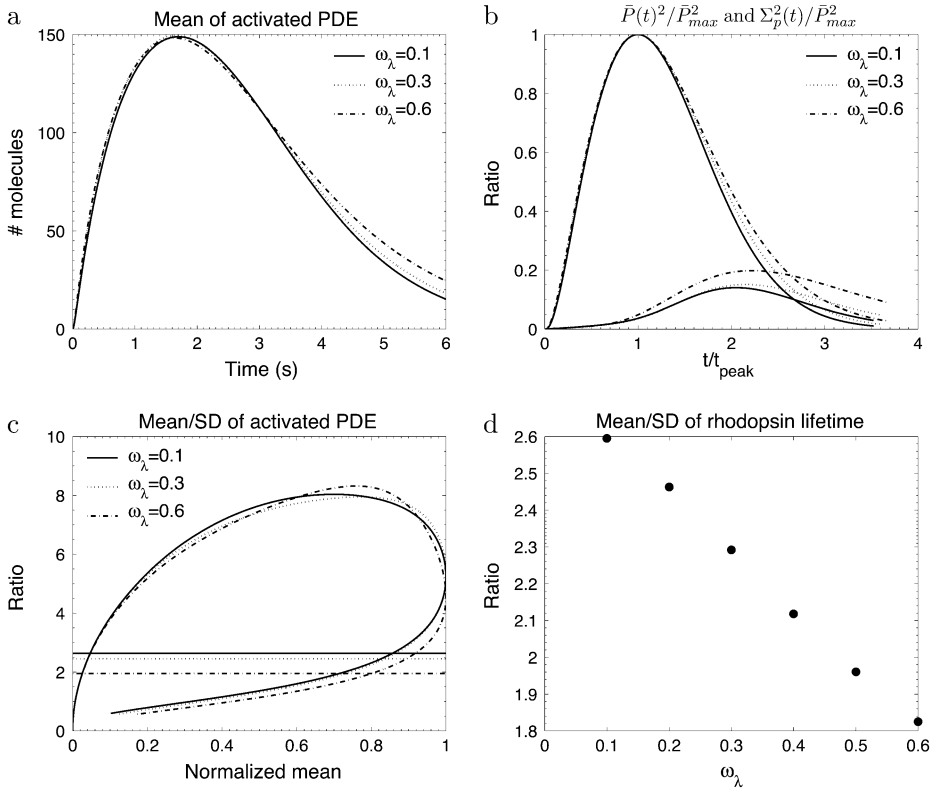

FIGURE 4 The simulations show the impact of the phosphorylation dependency of the rhodopsin phosphorylation rates for the toad rod scenario defined in Table 2. The behavior of the phosphorylation, arrestin binding, and transducin activation rates are given by Eqs. 48–50 with $\omega_{\text{act}} = 0.1$ and $N_{\text{p}} = 6$. For $\omega_\lambda = (0.1, 0.3, 0.6)$, the rates λ_{N} and $k_{\text{act}}(N)$ are given by (3.2, 6.8, 26.6) s^{-1} and (245, 273, 312) s^{-1}.

rhodopsin and the affinity increases linearly with the number of phosphorylations. Such a linear behavior was used for photoresponse simulations (18,19). However, experiments (15) have indicated that R* phosphorylation at three sites is needed to trigger arrestin binding with high affinity, which does not imply a gradual increase of the binding affinity. In addition, data obtained from transgenic mice lacking arrestin do not favor a gradual increase of the arrestin binding rates. Finally, there are no specific reasons to favor a linear decay of the arrestin binding affinity, while rhodopsin kinase and transducin affinities show an exponential profile.

To investigate the impact of arrestin binding on PDE* dynamics, we compare in Fig. 8 three arrestin binding scenarios called *optimal*, *exp*., and *linear*, obtained for toad rods with $N_{\text{P}} = 6$ and $\omega_{\text{act}} = \omega_\lambda = 0.1$: in the optimal scenario, arrestin binds only when R* is fully phosphorylated. In the linear scenario, the arrestin binding rates μ_{n} increase linearly with each phosphorylation step. Finally, in the scenario labeled by *exp*., the arrestin binding rates increase twofold with every phosphorylation step. To better compare these three scenarios, we chose the arrestin binding rates such that they reach the same maximal rate $\mu_{\text{N}} = 1.8\ \text{s}^{-1}$ when R* is fully phosphorylated. The simulations in Fig. 8 show that a linear increase leads to the highest PDE* variance and the lowest reliability ratio $R_{\text{P}}(t)$. This behavior is reasonable, since a linear increase also strongly affects the states before R* is fully phosphorylated. With an exponential increase, arrestin binding rates become predominant when R* is almost fully

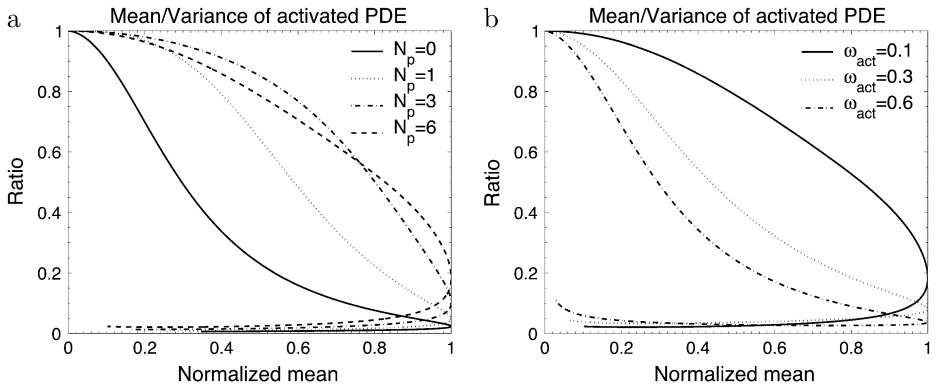

FIGURE 5 Mean/variance ratio of activated PDE. The simulations are obtained for the scenarios described in Fig. 2 and Fig. 3.

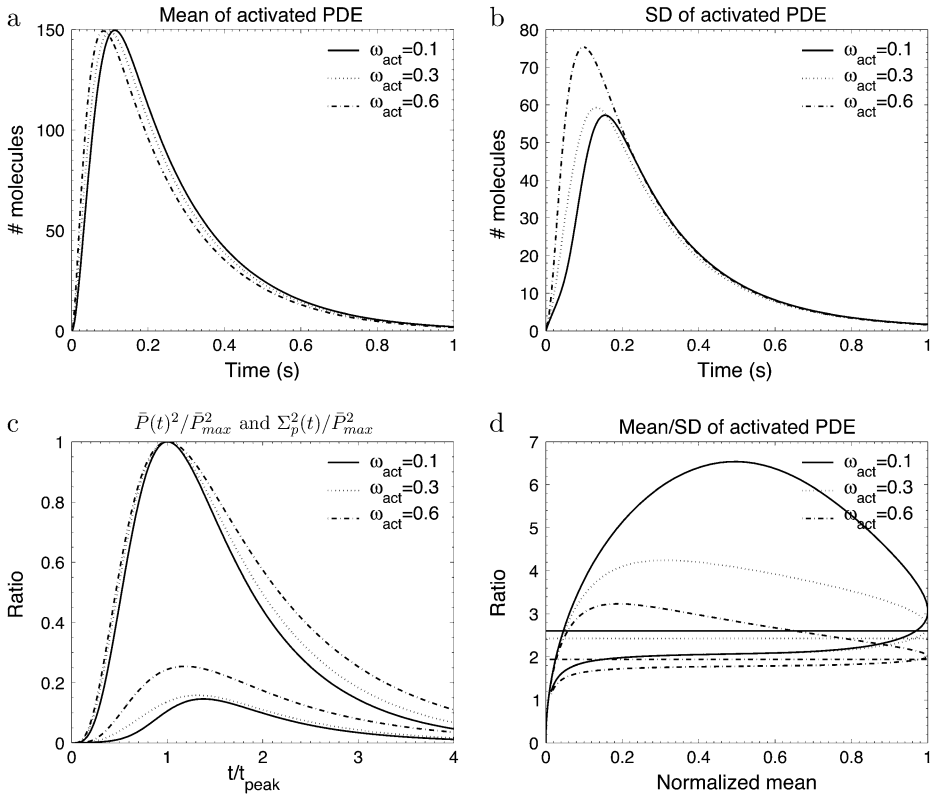

FIGURE 6 The simulations show the impact of the phosphorylation dependency of the transducin activation rates for the mouse rod scenario defined in Table 2. The behavior of the phosphorylation, arrestin binding, and transducin activation rates are given by Eqs. 48–50 with $\omega_\lambda = 0.1$ s and $N_p = 6$. For $\omega_{act} = (0.1, 0.3, 0.6)$, the rates λ_N and $k_{act}(N)$ are given by (120, 120, 120) s^{-1} and (3821, 6300, 10,242) s^{-1}.

phosphorylated, while they are relatively weak before. By comparing the simulations in Fig. 8 with the ones in Fig. 2, we deduce that large arrestin binding rates that come up already before R* has been fully phosphorylated have a similar impact to reducing the number of R* deactivation steps. For example, the curves in Fig. 8 for the *linear* scenario are similar to corresponding ones in Fig. 2 for $N_p = 1$. We conclude that for a given number of deactivation steps, linearly increasing arrestin binding rates are not efficient to achieve a high PDE activation reliability.

Only a few activated PDE molecules in cones

In cone photoreceptors, several synchronous photons have to be absorbed (10–12) to detect a signal out of the noise. For that reason, it is not possible to estimate experimentally the number of PDE* following a single photopigment excitation. Furthermore, due to experimental difficulties, many fundamental chemical constants are still missing for cones. A modeling approach is thus an unavoidable tool to investigate PDE activation in cones.

The origin of the background noise differs between L- and S-cones (12): in L-cones, a large spontaneous photopigment activation rate (12) constitutes the main source of the noise and this is a direct obstruction of a single photon detection. In contrast, the photopigment of S-cones is very stable and the background noise originates from spontaneous PDE activation (12,22).

Since spontaneous PDE activation is the main source of dark noise in rods and S-cones, we would like to investigate the question of why a single photon response can be observed in rods, but not in S-cones. A possible answer comes from biochemical data (38,39), which suggest that an excited photopigment presumably activates only very few PDE molecules. Biochemical results for carp cones (39) suggest that R* phosphorylation is much faster in cones compared to rods (~50 times faster), which seems to be caused by a higher rhodopsin kinase concentration and activity. Moreover, experimental data (39) also imply that the transducin activation rates are much smaller in cones compared to rods (~25 times smaller) and PDE deactivation is several times faster in cones compared to rods. This fast rate can be attributed to the higher RGS9 concentration (40,41).

To estimate the amount of PDE* molecules following a photopigment excitation, we have run various simulations. As expected, we found with no surprise that this amount is a decreasing function of PDE and R* deactivation (Fig. 9). The simulations presented in Fig. 9 are obtained by increasing the PDE* deactivation and R* phosphorylation rates of a toad rod by factors of 5, 10, and 15 (the parameters and simulations corresponding to the toad rod can be found in Fig. 2 for $N_p = 6$). We do not alter the transducin activation rates, but smaller transducin activation rates (as suggested in (39)) would additionally diminish the amount of PDE* in cones. Fig. 9 *a* shows that increasing the PDE* deactivation rate k_4 from 1 s^{-1} to 15 s^{-1} decreases the amount of PDE* from 150

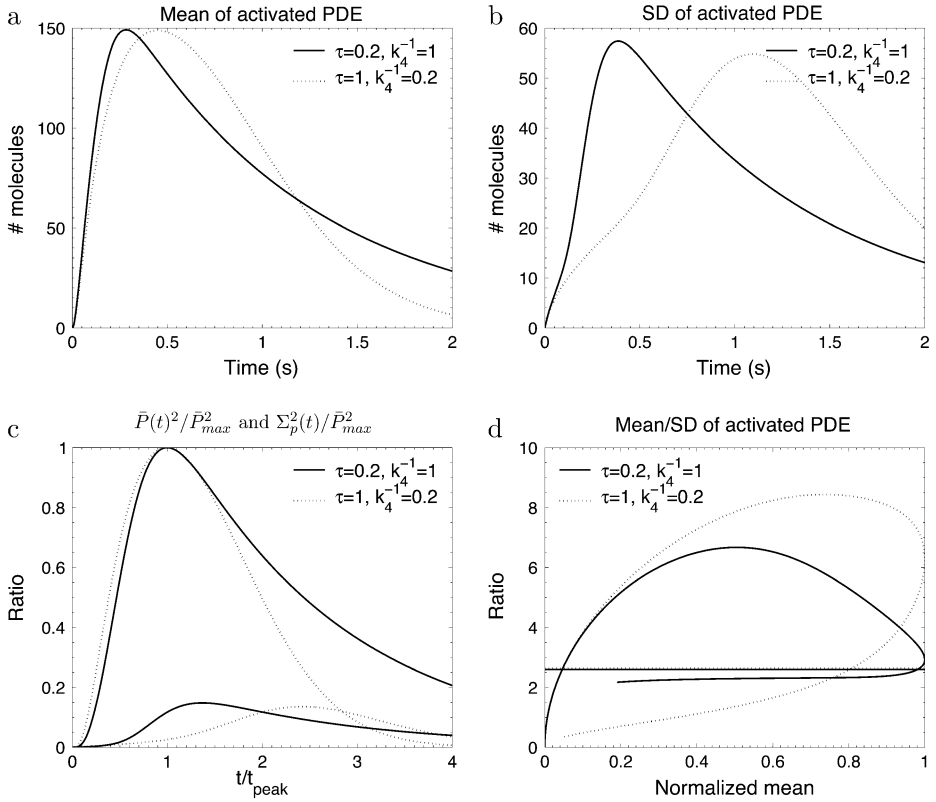

FIGURE 7 The simulations show the impact of interchanging the lifetimes of activated rhodopsin and PDE. The phosphorylation, arrestin binding, and transducin activation rates are given by Eqs. 48–50 with $\omega_\lambda = \omega_{\text{act}} = 0.1$, $N_\text{p} = 6$, $k_3 = 50\ \text{s}^{-1}$. For $\tau = (0.2, 1)$ s, the rates λ_N and $k_{\text{act}}(N)$ are (48.2, 9.6) s^{-1} and (1274, 1067) s^{-1}.

(amount for rod) to ~15. Since R* lifetime is not changed by increasing k_4, the recovery of the photoresponse is not affected. In Fig. 9 *b*, R* deactivation is enhanced. Compared to Fig. 9 *a*, this shows that a faster R* deactivation is less effective in diminishing the number of PDE* molecules. In Fig. 9 *b* PDE* deactivation becomes rate limiting ($k_4 = 1\ \text{s}^{-1}$) since R* lifetime is reduced from 3 s to 0.6 s, 0.3 s, and 0.2 s. Finally, in Fig. 9 *c*, PDE* and R* deactivation are increased simultaneously, which additionally reduces the amount of PDE*.

From our simulations we conclude that in cones, consistent with biochemical data (39), only very few PDE molecules are activated by an excited photopigment. This result can explain that for S-cones, contrary to rods, many synchronous photon absorptions are needed to produce a signal that overcomes the noise amplitude generated by spontaneous PDE activation.

DISCUSSION

We have studied here PDE activation by a single excited photopigment molecule using a Markov model and obtained explicit equations for the mean and the variance. This approach allowed us to investigate in detail the dynamics of PDE activation, which is indispensable and fundamental for the understanding of the photoresponse in rods and cones. Most experimental recordings are about the photocurrent, and today, unfortunately, there are no direct measurements of PDE activity, which is the main subject here. A full quantitative analysis of the photocurrent will imply to extend the model by including diffusible cGMP. Nevertheless, it is reasonable to assume that the photocurrent time course is largely determined by the one of activated PDE. In that case, our results can be connected to the photocurrent in two ways: first, to predict the photocurrent characteristics; and second, to infer from the observed photocurrent properties some of the unknown molecular details governing PDE activation.

Accurate rhodopsin deactivation does not necessarily lead to a reliable PDE activation

In rods the low variability of the photoresponse has been attributed mainly to the reliability of the lifetime of activated rhodopsin (13–16). In contrast, we have found that reliable PDE activation can be achieved even when rhodopsin lifetime is unreliable. To show this result, we estimated the reliability ratio R_τ (mean to standard deviation (SD)) of rhodopsin lifetime, and the reliability ratio R_{Ps} of the number of activated PDE during a SPR. We have found that the upper bound for both R_{Ps} and R_τ is $\sqrt{N_\text{p}+1}$ (N_p is the number of rhodopsin phosphorylation sites); however, maximal values for the ratios R_{Ps} and R_τ are in general not achieved simultaneously. R_{Ps} is maximal when all rhodopsin deactivation states have the same lifetime, whereas R_{Ps} becomes maximal

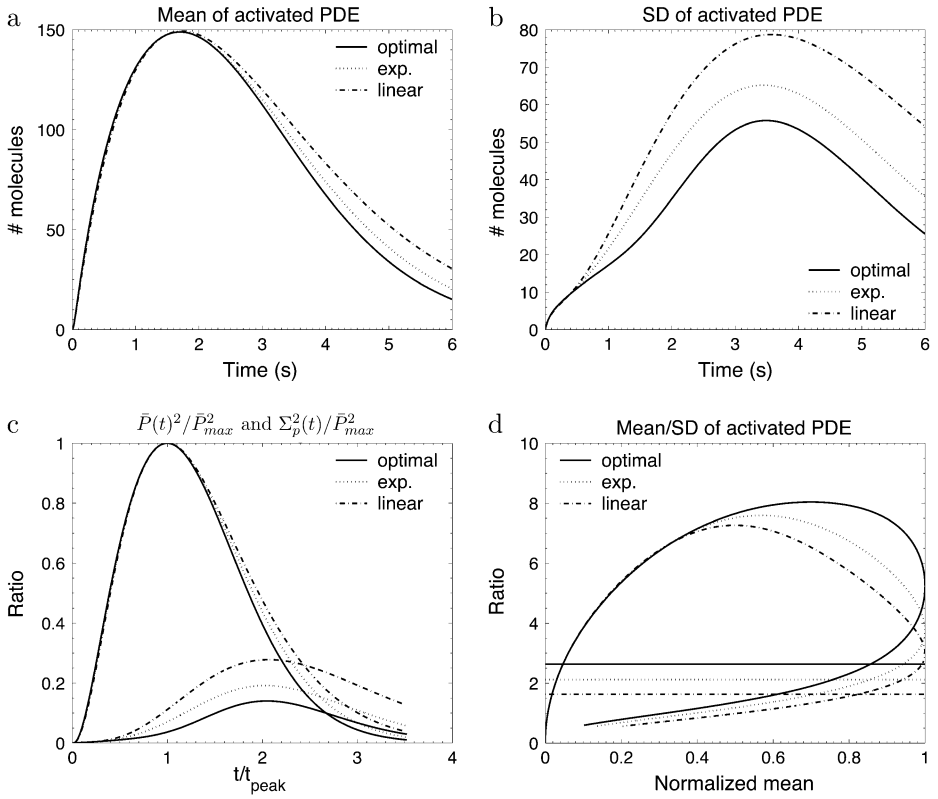

FIGURE 8 The simulations show the impact of different arrestin binding scenarios for the toad rod scenario defined in Table 2. The behavior of the phosphorylation and transducin activation rates are given by Eqs. 48 and 49 with $\omega_\lambda = \omega_{act} = 0.1$ and $N_p = 6$. In the *optimal* scenario, arrestin binds only when rhodopsin is fully phosphorylated and the rate is given by Eq. 50. In the *exp.* scenario, the arrestin binding rates increase twofold with each phosphorylation step according to $\mu_n = 1.8\ s^{-1}\ e^{-0.7(n-1)}$ for $n < N$ and $\mu_N = 0$. In the *linear* scenario, the arrestin biding rates increase linearly according to $\mu_n = (N - n)\ 0.3\ s^{-1}$. The arrestin binding rates are chosen such that in each scenario they reach the final value $\mu_1 = 1.8\ s^{-1}$. For the (*optimal*, *exp.*, *linear*) scenarios, the rates λ_N and $k_{act}(N)$ are given by (3.2, 2.05, 0.9) s^{-1} and (245, 237, 227) s^{-1}.

when in each state the same amount of PDE molecules are activated. Our results suggest that, in general, reliable rhodopsin deactivation and reliable PDE activation are not achieved simultaneously. In the literature, the focus is mainly on the reliability of rhodopsin deactivation, but one has to remember that the goal is not to reliably deactivate rhodopsin, but to reliably activate PDE.

In this work we assumed that each rhodopsin phosphorylation occurs through a single step and we did not investigate the effect of possible intermediate states, which implies that the number of rhodopsin deactivation states is given by $N = N_p + 1$. However, rhodopsin phosphorylation could proceed through additional intermediate steps (as was assumed in (18)). In such a case, the number of rhodopsin deactivation states N will become much larger than $N_p + 1$, which could significantly alter the variability of rhodopsin lifetime and activated PDE. In this context it is important to clarify whether rhodopsin activity in the intermediate states is zero or not. In Hamer et al. (18), the activity in intermediate states was assumed to be zero and so PDE activation occurred only in a much smaller subset of the deactivation states. However, it is also possible that rhodopsin activity persists in intermediate states, which can lead to a higher PDE activation reliability. In any case, with intermediate states the connection between the reliability of rhodopsin lifetime and PDE activation is less obvious, and it is possible to decouple the reliability of rhodopsin deactivation from the one of PDE activation.

High activation reliability during the rising phase

Our analysis revealed that the PDE variability is much smaller during the rising compared to the recovery phase (see, for example, Fig. 3). This finding agrees with similar observations for the photoresponse current (13,14,16). In particular, we have shown that during the rising phase the reliability ratio $R_P(t)$ reaches a maximum that can be much higher than the upper limit $\sqrt{N_P + 1}$ valid for R_τ or R_{Ps}. The rational behind this result is as follows: at the beginning, PDE variance closely equals the mean and therefore $R_P(t)$ rises like the square-root of the mean. For a large $R_P(t)$ maximum it is equally important that rhodopsin deactivates through many steps and the transducin activation rates decrease only slightly (not more than 10–20%) with subsequent phosphorylations (see Fig. 2 *e* and Fig. 3 *d*).

Biochemical data (28) indicate that the rhodopsin-transducin affinity decreases nearly twofold with each phosphorylation step, suggesting a similar decrease for the transducin activation rates. For the numerical simulations presented in Hamer et al. (18), the rhodopsin-transducin affinity was chosen to decrease nearly twofold with each phosphorylation step, in agreement with Gibson et al. (28). Nonetheless, since a reaction cascade with high backward reactions rates was used to model transducin activation, the effective transducin activation rates decreased much less than twofold. Taking into account the statement that phosphorylation was responsible for ~66% of the total rhodopsin activity reduction

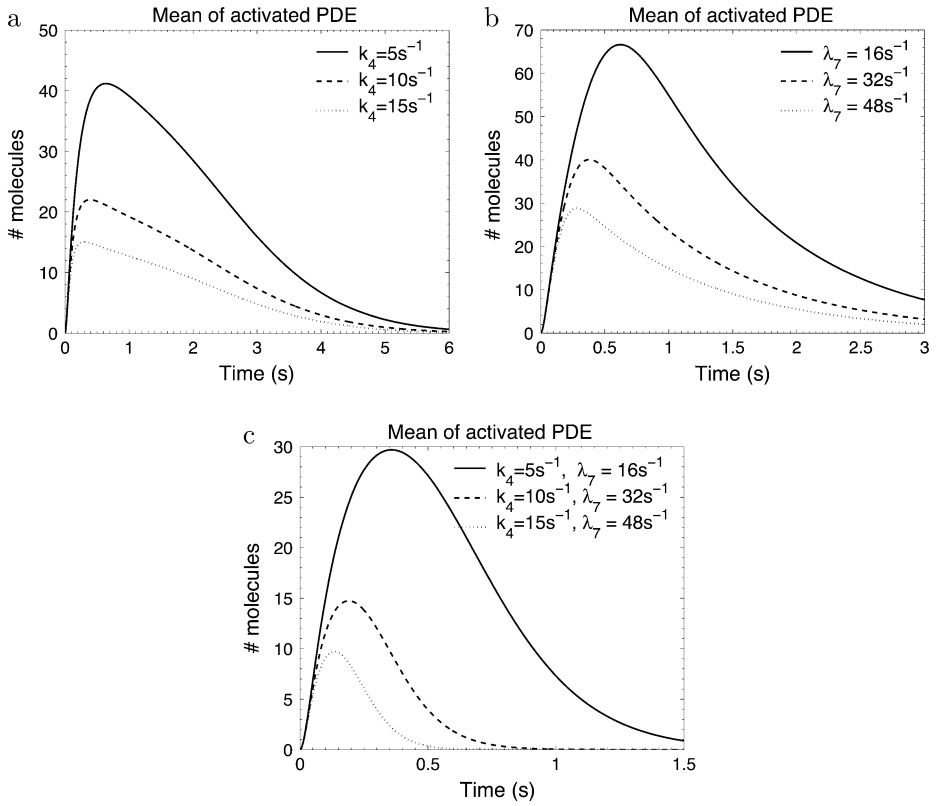

FIGURE 9 How to make a cone from a rod. The simulations show the mean PDE response for faster PDE and rhodopsin deactivation. The initial values for the rates are given in Fig. 2 for $N_p = 6$. In panel *a*, the PDE deactivation rate k_4 is increased from the initial value 1 s^{-1} by factors of 5, 10, and 15. In panel *b*, only the phosphorylation rate λ_7 is increased from the starting value 3.2 s^{-1} by factors of 5, 10, and 15. As a consequence, rhodopsin lifetime decreases from 3 s to 0.6 s, 0. 3 s, and 0.2 s. In panel *c*, k_4 and λ_7 are increased simultaneously.

(18), we estimated an effective decrease at ~14% with each phosphorylation step. Moreover, experimental results (27) indicate that rhodopsin's activity decreases in mouse rods through phosphorylation (at six phosphorylation sites) by ~50%, suggesting also subsequent decrease at ~10%. Finally, it is difficult to imagine that the transducin activation rates decrease by twofold with every phosphorylation step, since the activation rate would diminish to a very low value until rhodopsin is fully phosphorylated. In this case, the final rhodopsin shutoff through arrestin would be somehow obsolete and would barely change rhodopsin's activity, contrary to what is found (27).

A high activation reliability at peak time requires that rhodopsin deactivation limits recovery

The reliability ratio $R_P(t)$ at the time to peak depends crucially on whether rhodopsin or PDE deactivation is rate limiting (as illustrated in Fig. 7). If rhodopsin lifetime is much shorter than PDE lifetime, PDE deactivation can be neglected during the rising phase. In this case, the ratio $R_P(t)$ at time to peak and during the recovery phase is determined by the steady-state value R_{Ps}. Furthermore, since most of the PDE variance is generated by the activation process, the peak of the PDE mean and variance occur temporally close. In contrast, when rhodopsin lifetime is much larger than PDE lifetime, interesting dynamic effects show up. First, the ratio $R_P(t)$ at time to peak is no longer determined by R_{Ps} and can reach values that are much larger than $\sqrt{N_p + 1}$. Second, much of the PDE variance is now generated during the recovery phase which causes the variance to peak much later than the mean.

If the PDE variance determines the variance of the single photon response current and rhodopsin lifetime limits the photoresponse recovery, our results explain several experimental findings about the variance of the single photon response (14,16,17). Indeed, the measured coefficient of variation at the peak of the single photon response current, denoted by CV_{amp}, is found to be at ~0.2 and much less than the expected value $1/\sqrt{N_p + 1}$. Such a low value is predicted by the simulations in Fig. 2 *e*, where we found a value $R_P(t)$ at ~5 at peak time (since we expect that $CV_{amp}^{-1} \sim R_P(t)$ at peak time). Furthermore, experiments show that the variance of the single photon response peaks approximately twice later than the mean (14,16,17), which is similar to what we have found for the PDE variance in Fig. 2 *d*.

In mouse rods, PDE deactivation limits the recovery of the photoresponse (35). In that case, our analysis and the simulations in Fig. 6 *d* predict a value for CV_{amp} at $\sim 1/\sqrt{7} = 0.37$ ($N_p = 6$). In contrast, CV_{amp} in mouse rods is found to be ~0.2 (F. Rieke, 2007, personal communication), which is much too low to be explained by $R_P(t)$ at peak time. At this stage, it is not clear how CV_{amp} can become so small even when PDE lifetime limits the recovery. One possible explanation can be that the PDE variance is not representative for

the current variance, and including the cGMP-pathway might reveal more.

Number of activated PDE molecules during a single photon response

The maximum number of PDE molecules that are activated during the single photon response in rods seems to be an unresolved issue and indeed, a large discrepancy is found in the literature. For example, in Makino et al. (42) it was argued that >100 PDE molecules become activated. The numerical simulations presented in Hamer et al. (18) lead in average to 220 activated PDEs, and the rates provided in the literature (3,43,44) suggest a maximum value of <50. In contrast, based on noise analysis, it was suggested (45) that at least 2000 PDE molecules have to be active at peak time. Because of these large uncertainties, we decided to fix the maximum number of activated PDE at a value of 150. At this stage of our model, this choice has no important consequences, but it will become a serious issue for further investigations that include cGMP dynamics. Since the magnitude of cGMP hydrolysis depends on the number of activated PDE molecules, this quantitative question will have to be resolved to predict from molecular details the current of a photoresponse.

A related problem concerns the transducin activation rates. For amphibian rods, a value at $\sim 150\ s^{-1}$ was reported (37), while for mammalian rods a rate at $\sim 1300\ s^{-1}$ was provided (46). Because the rod photoresponse time course in mammalians is much faster compared to amphibians, this suggests that the transducin activation rates are regulated to ensure the activation of a reasonable amount of PDE molecules. For example, a transducin activation rate at $\sim 150\ s^{-1}$ would lead in mouse rods (where the rhodopsin lifetime seems to be <0.1 s (35)) to the activation of <10 PDE.

Only a few PDE molecules are activated by a excited photopigment in cones

Studying PDE activation in cones faces certain difficulties due to the limited amount of biochemical information available. However, by using the biochemical results for carp cones (39) as a guideline, our simulations (Fig. 9) suggest that only very few (<10) PDE molecules are activated by a single excited photopigment. This behavior would explain why in cones many quasisynchronous photon absorptions are needed to generate a signal that overcomes the background noise (10–12). In L-cones, the small amount of activated PDE is not an important issue, since already the large spontaneous photopigment activation rate (12) impedes the observation of a single photon absorption. However, in S-cones the photopigment is very stable (12) and, contrary to rods, the absorption of many photons seems to be necessary to activate sufficient PDE molecules that overcome the background noise set by spontaneous PDE activation.

APPENDIX

Mean and variance of the total number of PDE*

For $k_4 = 0$ and after R* shutoff, the number of PDE* reaches a steady-state value that accounts for all the PDE* activated during the response. Since every T* converts into a PDE*, the steady-state mean and variance of PDE* can be obtained by calculating the steady-state values of T* (for $k_3 = 0$). By setting $k_3 = 0$, integrating Eq. 24 from zero to infinity and using Eq. 21, we obtain the steady-state mean of T* and PDE* as

$$\bar{T}_s = \bar{P}_s = \int_0^\infty \bar{k}_{act}(t)dt = \sum_{i=1}^{N} \frac{k_{act}^{(i)}(N)}{\beta_i}. \tag{51}$$

Inserting the expressions for $k_{act}^{(i)}(N)$ in Eq. 19 yields the explicit solution

$$\bar{P}_s = \sum_{i=1}^{N} \frac{k_{act}^{(i)}(N)}{\beta_i} = \sum_{n=1}^{N} \frac{k_{act}(n)}{\beta_n} \prod_{k=n+1}^{N} p_k. \tag{52}$$

The steady-state variance of PDE* is obtained similarly from Eq. 31,

$$\Sigma^2_{T_s} = \Sigma^2_{P_s} = 2\int_0^\infty \Sigma^2_{k_{act}T}(t)dt + \bar{P}_s. \tag{53}$$

Using Eq. 34 and Eq. 39, the integral can be evaluated to give

$$\Sigma^2_{P_s} = \bar{P}_s + 2\sum_{i=1}^{N}\sum_{j=1}^{N} \frac{D_i^{(j)}(N)}{\beta_i\beta_j} - \bar{P}_s^2. \tag{54}$$

By using the formula (which can be derived by induction on N)

$$\sum_{i=1}^{N}\sum_{j=1}^{N} \frac{D_i^{(j)}(N)}{\beta_i\beta_j} = \sum_{i=1}^{N}\sum_{j=1}^{i} \frac{k_{act}(i)}{\beta_i}\frac{k_{act}(j)}{\beta_j} \prod_{k=j+1}^{N} p_k, \tag{55}$$

we finally get

$$\Sigma^2_{P_s} = \bar{P}_s + 2\sum_{i=1}^{N}\sum_{j=1}^{i} \frac{k_{act}(i)}{\beta_i}\frac{k_{act}(j)}{\beta_j} \prod_{k=j+1}^{N} p_k - \bar{P}_s^2. \tag{56}$$

Steady-state reliability ratio R_{Ps}

We now derive an upper limit for the steady-state ratio of the mean to the variance of PDE*, given by

$$R_{P_s} = \frac{\bar{P}_s}{\sqrt{\Sigma^2_{P_s}}} \le \frac{\sqrt{N}}{\sqrt{1 + \frac{N}{\bar{P}_s}}}. \tag{57}$$

To prove Eq. 57, we start from the Eq. 52 and Eq. 56 and introduce $x_i = k_{act}(i)/\beta_i$ and $\alpha_i = \prod_{k=i+1}^{N} p_k$. In terms of x_i and α_i, we get

$$\bar{P}_s = \sum_{i=1}^{N} x_i\alpha_i, \tag{58}$$

$$\Sigma^2_{P_s} = \bar{P}_s - \bar{P}_s^2 + 2\sum_{i=1}^{N}\sum_{j=1}^{i} x_i x_j \alpha_j. \tag{59}$$

Because Eq. 57 is equivalent to $N\Sigma^2_{P_s} - (\bar{P}_s^2 + N\bar{P}_s) \ge 0$, using Eq. 59 we have to show that

$$N\left(2\sum_{i=1}^{N}\sum_{j=1}^{i}x_i x_j\alpha_j-\sum_{i=1}^{N}\sum_{j=1}^{N}x_i x_j\alpha_i\alpha_j\right)-\bar{P}_s^2\geq 0. \quad (60)$$

For $\alpha_i \leq 1$, we have

$$2\sum_{i=1}^{N}\sum_{j=1}^{i}x_i x_j\alpha_j-\sum_{i=1}^{N}\sum_{j=1}^{N}x_i x_j\alpha_i\alpha_j\geq 2\sum_{i=1}^{N}\sum_{j=1}^{i}x_i x_j\alpha_i\alpha_j-\sum_{i=1}^{N}\sum_{j=1}^{N}x_i x_j\alpha_i\alpha_j=\sum_{i=1}^{N}x_i^2\alpha_i^2.$$

Finally, using the Cauchy-Schwarz inequality yields

$$\text{lhs. of Eq. 60}\geq N\sum_{i=1}^{N}x_i^2\alpha_i^2-\bar{P}_s^2=N\sum_{i=1}^{N}x_i^2\alpha_i^2-\left(\sum_{i=1}^{N}x_i\alpha_i\right)^2\geq 0, \quad (61)$$

which completes the proof.

The upper estimate for the ratio R_τ of R* lifetime is derived analogously to R_{Ps} by replacing $k_{act}(i)$ with 1. The result is

$$R_\tau=\frac{\tau}{\sqrt{\Sigma_\tau^2}}\leq\sqrt{N}. \quad (62)$$

Explicit expressions for the mean of T* and PDE*

Expressions for the mean of T* and PDE* are derived by integrating Eq. 24 and Eq. 25,

$$\bar{T}(t)=\sum_i k_{act}^{(i)}(N)\frac{e^{-\beta_i t}-e^{-k_3 t}}{k_3-\beta_i}, \quad (63)$$

$$\bar{P}(t)=\sum_i k_3\frac{k_{act}^{(i)}(N)}{k_3-\beta_i}\left(\frac{e^{-\beta_i t}-e^{-k_4 t}}{k_4-\beta_i}-\frac{e^{-k_3 t}-e^{-k_4 t}}{k_4-k_3}\right). \quad (64)$$

Small time asymptotic

To derive the small time asymptotic of the mean and the variance of PDE*, we use a Taylor expansion in Eq. 24 and Eq. 25 that leads to

$$\bar{T}(t)=\bar{k}_{act}(0)t+o(t^2)=k_{act}(N)t+o(t^2), \quad (65)$$

$$\bar{P}(t)=\frac{1}{2}k_3\bar{T}'(0)t^2+o(t^3)=\frac{1}{2}k_3k_{act}(N)t^2+o(t^3), \quad (66)$$

where $\bar{k}_{act}(0)=k_{act}(N)$. We conclude that for small time, the mean of PDE* rises like t^2, in contrast with the linear asymptotic result proposed in the literature (1,23), where PDE activation by T* was considered to occur instantaneously. Using again a Taylor expansion in Eqs. 31–33 and in Eqs. 35 and 36, we find the small time asymptotic for the variance of T* and PDE* as

$$\Sigma_T^2(t)=\bar{T}(t)+\frac{1}{3}\beta_N k_{act}(N)^2\gamma_N t^3+o(t^4), \quad (67)$$

$$\Sigma_P^2(t)=\bar{P}(t)+\frac{1}{20}k_3^2\beta_N k_{act}(N)^2\gamma_N t^5+o(t^6), \quad (68)$$

where $\beta_N=\lambda_N+\mu_N$ and

$$\gamma_N=\left(1-\frac{k_{act}(N-1)}{k_{act}(N)}\right)^2. \quad (69)$$

For small time asymptotic, the variance of T* and PDE* equal the mean. Since all parameters in Eq. 68 and Eq. 67 are positive, the variance cannot be smaller than the mean and becomes minimal for $\gamma_N=0$ ($k_{act}(N)=k_{act}(N-1)$). In that case, when R* undergoes a transition from the state N to $N-1$, the activation rate does not change and therefore does not generate any additional source of variability. The variance becomes also minimal for $\beta_N=0$, that is when activated rhodopsin is stable. In this case, transducin activation proceeds as a Poisson process.

We now estimate the small time asymptotic of the reliability ratio $R_P(t)$, defined in Eq. 40. Using Eq. 66 and Eq. 68, we obtain

$$R_P(t)=\sqrt{\bar{P}(t)}\left(1-\frac{1}{20}k_3\beta_N k_{act}(N)\gamma_N t^3+o(t^4)\right). \quad (70)$$

For small time, $R_P(t)$ rises proportional to $\sqrt{\bar{P}(t)}$, while for larger times, the second term in Eq. 70 becomes predominant and thus attenuates the rising of $R_P(t)$. Moreover, for $\gamma_N=0$, the ratio $R_P(t)$ in Eq. 70 becomes maximal and the duration of the rising phase is prolonged.

Mathematical identities

The following identities are true for all N real numbers β_k:

$$\sum_{i=1}^{N}\prod_{\substack{k=1\\k\neq i}}^{N}\frac{\beta_k}{\beta_k-\beta_i}=1, \quad (71)$$

$$\sum_{j=1}^{N}\frac{1}{\beta_j}\prod_{\substack{k=1\\k\neq j}}^{N}\frac{\beta_k}{\beta_k-\beta_j}=\sum_{j=1}^{N}\frac{1}{\beta_j}. \quad (72)$$

These formulas can be derived by induction on the number N.

D.H.'s research is supported by the program ''Chaire d'Excellence''.

REFERENCES

1. Pugh, E., Jr., and T. Lamb. 1993. Amplification and kinetics of the activation steps in phototransduction. *Biochim. Biophys. Acta.* 1141: 111–149.
2. Rieke, F., and D. Baylor. 1998. Single photon detection by rod cells of the retina. *Rev. Mod. Phys.* 70:1027–1036.
3. Pugh, E., Jr., and T. Lamb. 2000. Phototransduction in vertebrate rods and cones: molecular mechanism of amplification, recovery and light adaptation. *In* Handbook of Biological Physics. Elsevier, Dordrecht, The Netherlands.
4. Burns, M., and D. Baylor. 2001. Activation, deactivation, and adaptation in vertebrate photoreceptor cells. *Annu. Rev. Neurosci.* 24:779–805.
5. Arshavsky, V., T. Lamb, and E. Pugh, Jr. 2002. G-proteins and phototransduction. *Annu. Rev. Physiol.* 64:153–187.
6. Burns, M., and V. Arshavsky. 2005. Beyond counting photons: trials and trends in vertebrate visual phototransduction. *Neuron.* 48:387–401.
7. Hecht, S., S. Shlaer, and M. Pirenne. 1942. Energy, quanta and vision. *J. Gen. Physiol.* 25:819–840.
8. Sakitt, B. 1972. Counting every quantum. *J. Physiol.* 223:131–150.
9. Baylor, D., T. Lamb, and K.-W. Yau. 1979. Responses of retinal rods to single photons. *J. Physiol.* 288:613–634.
10. Schnapf, J., B. Nunn, M. Meister, and D. Baylor. 1990. Visual transduction in cones of the monkey *Macaca fascicularis*. *J. Physiol.* 427:681–713.

11. Miller, J., and J. Korenbrot. 1993. Phototransduction and adaptation in rods, single cones, and twin cones of the striped brass retina: a comparative study. *Vis. Neurosci.* 10:653–667.
12. Rieke, F., and D. Baylor. 2000. Origin and functional impact of dark noise in retinal cones. *Neuron.* 26:181–186.
13. Doan, T., A. Mendez, P. Detwiler, J. Chen, and F. Rieke. 2006. Multiple phosphorylation sites confer reproducibility of the rod's single-photon responses. *Science.* 13:530–533.
14. Field, G., and F. Rieke. 2002. Mechanisms regulating variability of the single photon responses of mammalian rod photoreceptors. *Neuron.* 35: 733–747.
15. Mendez, A., M. Burns, A. Roca, J. Lem, L. Wu, M. Simon, D. Baylor, and J. Chen. 2000. Rapid and reproducible deactivation of rhodopsin requires multiple phosphorylation sites. *Neuron.* 28:153–164.
16. Whitlock, G., and T. Lamb. 1999. Variability in the time course of single photon responses from toad rods: termination of rhodopsin's activity. *Neuron.* 23:337–351.
17. Rieke, F., and D. Baylor. 1998. Origin of reproducibility in the responses of retinal rods to single photons. *Biophys. J.* 75:1836–1857.
18. Hamer, R., S. Nicholas, D. Tranchina, P. Liebman, and T. Lamb. 2003. Multiple steps of phosphorylation of activated rhodopsin can account for the reproducibility of vertebrate rod single-photon responses. *J. Gen. Physiol.* 122:419–444.
19. Hamer, R., S. Nicholas, D. Tranchina, T. Lamb, and J. Jarvinen. 2005. Toward a unified model of vertebrate rod phototransduction. *Vis. Neurosci.* 22:417–436.
20. Lamb, T. 1994. Stochastic simulation of activation in the G-protein cascade of phototransduction. *Biophys. J.* 67:1439–1454.
21. Felber, S., H. Breuer, F. Petruccione, J. Honerkamp, and K. Hofmann. 1996. Stochastic simulation of the transducin GTPase cycle. *Biophys. J.* 71:3051–3056.
22. Holcman, D., and J. Korenbrot. 2005. The limit of photoreceptor sensitivity: molecular mechanism of dark noise in retinal cones. *J. Gen. Physiol.* 125:641–660.
23. Pugh, E., Jr., and T. Lamb. 1992. A quantitative account of the activation steps involved in phototransduction in amphibian photoreceptors. *J. Physiol.* 449:719–758.
24. Wilden, U., and H. Kühn. 1982. Light-dependent phosphorylation of rhodopsin: number of phosphorylation sites. *Biochemistry.* 21:3014–3022.
25. Wilden, U. 1995. Duration and amplitude of the light induced multiple phosphorylation of rhodopsin: number of phosphorylation sites. *Biochemistry.* 34:1446–1454.
26. Chen, J., C. Makino, N. S. Peachey, D. A. Baylor, and M. I. Simon. 1995. Mechanisms of rhodopsin inactivation in vivo as revealed by a COOH-terminal truncation mutant. *Science.* 267:374–377.
27. Xu, J., R. Dodd, C. Makino, M. I. Simon, D. A. Baylor, and J. Chen. 1997. Prolonged photoresponses in transgenic mouse rods lacking arrestin. *Nature.* 389:505–509.
28. Gibson, S., J. Parkes, and P. Liebman. 2000. Phosphorylation modulates the affinity of light-activated rhodopsin for G-protein and arrestin. *Biochemistry.* 39:5738–5749.
29. Chen, C.-K., M. E. Burns, W. He, T. G. Wensel, D. A. Baylor, and M. I. Simon. 2000. Slowed recovery of rod photoresponse in mice lacking the GTPase accelerating protein RGS9-1. *Nature.* 403:557–560.
30. Lishko, P., K. Martemyanov, J. Hopp, and V. Arshavsky. 2002. Specific binding of RGS9-Gβ5l to protein anchor in photoreceptor membranes greatly enhances its catalytic activity. *J. Biol. Chem.* 277: 24376–24381.
31. Lyubarsky, A., C.-K. Chen, F. Naarendorp, X. Zhang, T. Wensel, M. Simon, and E. Pugh, Jr. 2001. RGS9-1 is required for normal inactivation of mouse cone phototransduction. *Mol. Vis.* 7:71–78.
32. He, W., C. Cowan, and T. Wensel. 2006. RGS9, a GTPase accelerator for phototransduction. *Neuron.* 51:409–416.
33. Schuss, Z. 1980. Theory and Applications of Stochastic Differential Equations. Wiley Series in Probability and Statistics. John Wiley & Sons, New York.
34. Gardiner, C. 2003. Handbook of Stochastic Methods, 3rd Ed. Springer, New York.
35. Krispel, C., D. Chen, N. Melling, Y. Chen, K. Martemyanov, N. Quillinan, T. Arshavsky, V. Y. Wensel, C. Chen, and M. Burns. 2006. RGS expression rate-limits recovery of rod photoresponses. *Neuron.* 51:409–416.
36. Imai, H., V. Kefalov, K. Sakurai, O. Chisaka, Y. Ueda, A. Onishi, T. Morizumi, Y. Fu, K. Ichikawa, K. Nakatani, Y. Honda, J. Chen, K.-W. Yau, and Y. Shichida. 2007. Molecular properties of rhodopsin and rod function. *J. Biol. Chem.* 282:6677–6684.
37. Leskov, I., V. Klenchin, J. Handy, G. Whitlock, V. Govardovskii, M. Bownds, T. Lamb, E. Pugh, Jr., and V. Arshavsky. 2000. The gain of rod phototransduction: reconciliation of biochemical and electrophysiological measurements. *Neuron.* 27:525–537.
38. Tachibanaki, S., S. Tsushima, and S. Kawamura. 2001. Low amplification and fast visual pigment phosphorylation as mechanisms characterizing cone photoresponses. *Proc. Natl. Acad. Sci. USA.* 98:14044–14049.
39. Tachibanaki, S., Y. Shimauchi-Matsukawa, D. Arinobu, and S. Kawamura. 2007. Molecular mechanism characterizing cone photoresponses. *Photochem. Photobiol.* 83:19–26.
40. Zhang, X., T. Wensel, and T. Kraft. 2003. GTPase regulators and photoresponses in cones of the Eastern chipmunk. *J. Neurosci.* 23: 1287–1297.
41. Cowan, C., R. Fariss, I. Sokal, K. Palczewski, T. Wensel, M. Simon, and E. Pugh, Jr. 1998. High expression levels in cones of RGS9, the predominant GTPase accelerating protein of rods. *Proc. Natl. Acad. Sci. USA.* 95:5351–5356.
42. Makino, C., X. Wen, and J. Lem. 2003. Piecing together the timetable for visual transduction with transgenic animals. *Curr. Opin. Neurobiol.* 13:404–412.
43. Caruso, G., H. Khanal, V. Alexiadis, F. Rieke, H. Hamm, and E. DiBenedetto. 2005. Mathematical and computational modeling of spatio-temporal signaling in rod phototransduction. *IEEE Proc. Syst. Biol.* 153:119–137.
44. Nikonov, S., T. Lamb, and E. Pugh, Jr. 2000. The role of steady phosphodiesterase activity in the kinetics and sensitivity of the light-adapted salamander rod photoresponse. *J. Gen. Physiol.* 116:795–824.
45. Rieke, F., and D. Baylor. 1996. Molecular origin of continuous dark noise in rod photoreceptors. *Biophys. J.* 71:2553–2572.
46. Heck, M., and K. Hofmann. 2001. Maximal rate and nucleotide dependence of rhodopsin-catalyzed transducin activation. *J. Biol. Chem.* 276: 10000–10009.